CAMPYLOBACTER JEJUNI 1291 IN CELL MORPHOLOGY AND PATHOGENESIS

by

Jennifer Dechka

B.Sc. with distinction, University of Victoria, 2019

A THESIS SUBMITTED IN PARTIAL FULFILLMENT OF

THE REQUIREMENTS FOR THE DEGREE OF

MASTER OF SCIENCE

in

THE FACULTY OF GRADUATE AND POSTDOCTORAL STUDIES

(Microbiology and Immunology)

THE UNIVERSITY OF BRITISH COLUMBIA

(Vancouver)

December 2022

The following individuals certify that they have read, and recommend to the Faculty of Graduate and Postdoctoral Studies for acceptance, the thesis entitled:

Campylobacter jejuni 1291 in cell morphology and pathogenesis

submitted by Jennifer Dechka in partial fulfilment of the requirements for

the degree of Master of Science

in Microbiology and Immunology

Examining Committee:

Dr. Erin Gaynor, Professor, Microbiology & Immunology, UBC
Supervisor

Dr. Michael Murphy, Professor, Department Head, Microbiology & Immunology, UBC
Supervisory Committee Member

Dr. Rosemary Redfield, Emerita, Zoology, UBC
Additional Examiner

Additional Supervisory Committee Members:

Dr. B. Brett Finlay, Professor, Microbiology & Immunology, Biochemistry & Microbiology, UBC
Supervisory Committee Member

Abstract

Campylobacter jejuni is a widespread enteric pathogen that causes mild to severe gastroenteritis in humans. Despite the prevalence of *C. jejuni*, its virulence mechanisms are poorly understood. It had long been postulated that *C. jejuni*'s characteristic helical shape was important for pathogenesis, which our group has now shown to be the case. Peptidoglycan remodelling enzymes play a key role in maintaining cell shape. The LytM domain-containing protein *1291* was identified while searching the *C. jejuni* genome for peptidoglycan peptidases. As 1291 was predicted to lack proteolytic activity, it was subsequently predicted to activate the *C. jejuni* amidase, AmiA. Deletion of *1291* caused distinct phenotypic changes compared to wild type *C. jejuni*. The *1291* deletion mutant demonstrated a long chain-like cellular morphology similar to an *amiA* deletion strain and contributed to key pathogenesis phenotypes. In comparison to wild type, Δ*1291* displayed severe motility and autoagglutination defects, as well as an increase in biofilm formation. Both 1291 and the *E. coli* LytM domain-containing amidase activator EnvC showed cross-species complementation. Specifically, 1291 was able to complement the severe chaining phenotype of an *E. coli* amidase activator deletion strain, and EnvC was able to complement the chain-like phenotype of Δ*1291*. This work provides evidence that 1291 acts as a pathogenesis factor in *C. jejuni* and is involved in cellular morphological changes, likely through the activation of *C. jejuni*'s sole amidase, AmiA.

Lay Summary

Campylobacter jejuni is often the leading cause of food-borne bacterial diarrheal disease, known as campylobacteriosis, in developed countries. Though campylobacteriosis is prevalent, *C. jejuni*'s pathogenesis mechanisms are poorly understood as it lacks common virulence factors seen in other enteric pathogens like *Escherichia coli* and *Salmonella* spp. *C. jejuni*'s characteristic helical cell shape was recently identified as critical for human pathogenesis: the loss of enzymes that modify peptidoglycan, a rigid structural component of the bacterial cell wall, caused changes to the helical cell morphology and led to a reduction in pathogenesis and virulence attributes. This research aims to further understand the connection between cell shape determinants and pathogenesis in *C. jejuni* by investigating the interaction between a known peptidoglycan-modifying enzyme, AmiA, and its potential activator protein, 1291. This research will contribute to a growing database of *C. jejuni* morphology factors which can be utilized in future development of pathogen control strategies.

Preface

The overall project was designed by Dr. E. Gaynor, Dr. E. Frirdich, and me. Prior to the start of the project, Dr. E. Frirdich and J. Wallace identified the gene *1291* when searching the *C. jejuni* genome for proteins containing peptidase domains. Dr. E. Frirdich and J. Wallace used STRING analysis to determine that 1291 and AmiA showed cooccurrence and found gene domain homology between 1291 and the LytM domain-containing proteins EnvC and NlpD from both *Escherichia coli* and *Vibrio cholerae*. All additional bioinformatic analyses were done by me.

The *C. jejuni* strain 81-176 is the wild type strain used in our lab. The initial Δ*1291* strain and the *1291*_pRRC plasmid were constructed by J. Wallace. I constructed all strains designated "this study" in Tables 2.1 and 3.1. The *E. coli* strains used in Chapter 3 (TB28, TB134, TB139, and TB156), were generously provided by Dr. T. G. Bernhardt and his lab at Harvard Medical School. J. Wallace organized shipment of the *E. coli* strains, and I made stock cultures from the samples sent. In Tables 2.2 and 3.2, all primers designated "in house" were designed by J. Wallace, except aphA3-1 which was designed by Dr. E. Frirdich, and all primers designated "this study" were designed by me.

All phenotype assays described in Chapter 2 are standard to the Gaynor lab, except for the hydrophobicity assay, which I adapted for use in this project. All assays in Chapter 2 were performed by me. The cross-complementation study described in Chapter 3 was designed and performed by me. Research data analysis was completed by me with feedback from Dr. E. Gaynor, Dr. E. Frirdich, Dr. A. Lin, and J. Wallace.

Table of Contents

List of Tables

List of Figures

List of Abbreviations

α	Alpha
β	Beta
Δ	Deletion
Δ*1291*c	*1291* complemented mutant
Δ*1291*	*1291* deletion strain
Δ*envC*	*E. coli envC* deletion strain
Δ*envC*Δ*nlpD*	*E. coli envC* and *nlpD* deletion strain
Δ*nlpD*	*E. coli nlpD* deletion strain
Ω	Ohm
µg	Micrograms
µl	Microlitres
µF	Microfarad
1291CO	Codon optimized version of *1291*
*1291*OE	*1291* overexpressing strain
81-176	*Campylobacter jejuni* wild type strain used in this study
A_{570nm}	Absorbance at 570 nm
Ala	Alanine
ANOVA	Analysis of variance
aphA3	Non-polar kanamycin resistance cassette
Approx.	Approximately
Ap^R	Ampicillin resistant
BHI	Brain heart infusion
BLAST	Basic local alignment search tool
bp	Base pairs
˚C	Celsius
cat	Chloramphenicol acetyltransferase
CFU	Colony forming unit
CFW	Calcofluor-white
Cj	*Campylobacter jejuni*
Cm	Chloramphenicol
Cm^R	Chloramphenicol resistant

CO_2	Carbon dioxide
dH_2O	Distilled water
DIC	Direct interference contrast
DMSO	dimethyl sulfoxide
DNA	Deoxyribonucleic acid
eDNA	Extracellular DNA
EtOH	Ethanol
E value	Expect value
g	Grams
gDNA	Genomic DNA
Glc*N*Ac	*N*-acetylglucosamine
HPLC	High-performance liquid chromatography
hr	Hours
iGlu	Isoglutamic acid
IL-8	Interleukin-8
Km	Kanamycin
Km^R	Kanamycin resistant
LB	Luria-Bertani media
LOS	Lipooligosaccharide
LytM	Lysostaphin-like metalloendopeptidase domain, also known as M23 peptidase domain
M23	Domain belonging to M23 family of metalloendopeptidases, also known as LytM domain
Mb	Mega base pairs
meso-Dap	*Meso*-diaminopimelic acid
mg	Milligrams
MH	Mueller-Hinton media
MH-TV	Mueller-Hinton supplemented with trimethoprim and vancomycin
min	Minutes
ml	Millilitres
mm	Millimetres
Mur*N*Ac	*N*-acetylmuramic acid
N-linked	Nitrogen-linked

NF-κB	Nuclear factor kappa B
ng	Nanograms
nm	Nanometres
Nod	Nucleotide-binding oligomerization domain
O_2	Oxygen
O-linked	Oxygen-linked
OD	Optical density
p	Probability
PBS	Phosphate-buffered saline
PCR	Polymerase chain reaction
PG	Peptidoglycan
qPCR	Quantitative PCR
RBS	Ribosomal binding site
rcf	Relative centrifugal force
RNA	Ribonucleic acid
RNaseA	Ribonuclease A
rpm	Revolutions per minute
rRNA	Ribosomal RNA
RT	Room temperature
s.d.	Standard deviation
SDS-PAGE	Sodium dodecyl sulfate-polyacrylamide gel electrophoresis
TB28	*E. coli* wild type strain used in this study
TLR	Toll-like receptor
UV	Ultraviolet
V	Voltage
w/v	Weight/volume ratio
WT	Wild type

Acknowledgements

Firstly, I acknowledge that I completed my master's degree on the traditional, ancestral, and unceded territory of the xʷməθkʷəy̓əm (Musqueam) First Nation.

I am exceptionally grateful to Dr. Erin Gaynor and the Gaynor lab for welcoming me into the lab and supporting me throughout my graduate school journey. I thank Dr. Gaynor for continued encouragement and sharing her scientific wisdom, Dr. Emilisa Frirdich for invaluable help with troubleshooting and experimental design, and Jenny Wallace for extensive technical help and support.

I thank my committee members, Dr. Michael Murphy, and Dr. Brett Finlay for giving me valuable and constructive feedback over the course of my degree, and Dr. Murphy and Dr. Rosie Redfield for agreeing to be my examiners and for thoroughly evaluating my work. Thanks are also owed to Dr. Thomas Bernhardt and his lab at Harvard Medical School for graciously providing the *Escherichia coli* strains used in Chapter 3, and to Dr. Murphy and his lab for equipment usage.

I offer my gratitude to all the LSI staff, including the custodians, maintenance, IT, and administration, especially Gilly Veniegas, and Dr. John "NOMO" Nomellini, who are truly the backbone of the second floor. I am also vastly appreciative of the guidance and support I received from the Graduate Program Manager, Darlene Birkenhead.

I am grateful for the tuition funding I received from the Canadian Institutes of Health Research Canada Graduate Scholarship Master's Award (2021), as well as the tuition funding I received from my parents.

An extremely big thank you is owed to Mama and Papa, for moral support, prepped meals, and for picking up the phone every time I called. Thank you to my little-dog-brother Kona for all the cuddles and emotional support, especially while writing this thesis, and for being happy to see

me each time I came home from Vancouver. Other overly large thanks go to my cheerleaders: Amy, Sara, Melissa, Lauren, Naomi, and Karina. I am also very thankful for the support given to me by Darcy, Rike, and Alysha. Grad school was a lot easier knowing you were all there behind me. I give thanks to Monty Python, Classic FM, Little Mix, Charlene Kaye, Stephen Fry and Formula 1, for picking me up when I felt uninspired and for always giving me something to look forward to.

Finally, I acknowledge all the hard work I put into this project, especially when it was not running smoothly, as I am proud of my accomplishments during my time at the University of British Columbia.

To Eric Idle

Chapter 1: Introduction

1.1 *Campylobacter jejuni*

Campylobacter jejuni (*Cj*) is a Gram-negative, highly motile epsilon proteobacterium. *Cj* is microaerophilic, capnophilic, and thermophilic with growth temperatures between 37-42˚C, but perhaps its most distinct physical characteristic is its helical shape. *Cj* is often the leading cause of food-borne bacterial diarrheal disease in humans in developed countries (1). Infection with *Cj*, known as campylobacteriosis, commonly causes mild to severe watery or bloody diarrhea and can lead to hospitalization or death in old, young, and immunocompromised patients, though the infection is typically self-limiting (1). The onset of campylobacteriosis can occur as early as 17 hours post-ingestion of as few as 800 bacteria and can last from days to weeks (2-4). During human infection, *Cj* colonizes and adheres to the epithelial cells of the large intestine where it can replicate to concentrations as high as 3.0×10^8 colony forming units (CFU) per gram of fecal material (3). It can also invade and survive within intestinal epithelial cells, which is postulated to contribute to virulence (5-7). Following infection and colonization of the intestinal tract, *Cj* can trigger a variety of human innate immune responses including activation of the transcription factor, NF-κB (8, 9), which mediates the production of chemokines and cytokines such as the neutrophil chemoattractant interleukin 8 (IL-8) (10, 11), as well as inducing dendritic cell maturation (12, 13).

In some cases, campylobacteriosis can result in severe sequelae including reactive arthritis, inflammatory bowel diseases like Crohn's disease, ulcerative colitis and colorectal cancer, and autoimmune inflammatory demyelination diseases such as Guillain-Barré and Miller Fisher syndromes (14-17). Prolonged *Cj* intestinal colonization has also been associated with the onset of intestinal mucosa-associated lymphoid tissue lymphoma (18).

Though *Cj* can cause severe disease in humans, it lives commensally in the digestive tracts of wild and domestic animals, particularly avian species (19-22). In poultry, *Cj* colonizes two blind pouches at the junction of the small and large intestines called the ceca. Here, colonies can replicate to concentrations of 2.5×10^9 CFU/g of cecal material without adverse effects on the host (23, 24). Drinking water can also become contaminated with *Cj* and lead to community outbreaks such as occurred in Walkerton, Ontario (25). Thus, most instances of campylobacteriosis in humans arise from ingestion of contaminated poultry, water or unpasteurized milk, or food cross-contaminated with raw poultry juice (1, 26, 27).

1.2 *C. jejuni* lacks canonical bacterial virulence factors

Common virulence factors in other enteric pathogens like pili, and enterotoxins are absent in *Cj* (28, 29). Canonical type III secretion systems are absent in *Cj* as well, although the flagellar export apparatus has been shown to act as a type III secretion system (29-31). The *Cj* flagellin is also a very poor stimulator of human toll-like receptor 5 (TLR-5), a receptor expressed in intestinal epithelial cells that recognizes bacterial flagella and to stimulates proinflammatory cytokine production (32). This was shown as the purified *Cj* flagellar protein FlaA was unable to induce cytokine production in cultured epithelial cells or in inoculated mice (32).

Some factors important for pathogenesis that are present in other gastrointestinal pathogens are missing or limited in *Cj*. Though many classic stress response elements like the stationary phase sigma factor RpoS are absent, *Cj* does have a stringent response modulator, SpoT (29, 33, 34). *Cj* is also lacking the oxidative stress proteins SoxRS and OxyR which are seen in many Gram-negative pathogens; however, it does possess a peroxide sensing PerR regulator, which is described further below (34, 35). Direct DNA repair genes, SOS response genes, and glycosylases

involved in DNA repair studied in *Escherichia coli* are absent from the *Cj* genome (29). *Cj* also lacks a functional DNA mismatch repair system to correct replication errors from single base pair mismatches and slipped-strand mispairing arising from homopolymeric regions, which could lead to increases in mutation rates and phase variation within a strain as described further below (29, 36).

1.3 *C. jejuni* pathogenesis factors

Since *Cj* is lacking many common pathogenesis strategies, basic cellular processes are hypothesized to be important contributors to disease etiology (33, 34, 37). *Cj* is relatively fragile to work with in the laboratory, requiring fastidious atmospheric and nutrient conditions for growth (38). However, as *Cj* is able to survive in multiple different *in vivo* and *ex vivo* environments, mechanisms involved in stress survival, metabolism, and colonization will in turn affect the organism's ability to cause disease in humans (39).

The *Cj* genome is relatively small (approx. 1.6 Mb); however, it encodes multiple hypervariable regions containing short runs of homopolymeric poly-G, poly-C (29), and poly-A (40, 41) nucleotides which are prone to a high rate of slip-strand mispairing due to a lack of DNA mismatch repair genes (29, 42). These regions result in a high rate of phase variation which leads to a large degree of both genetic and phenotypic variation between *Cj* strains, likely conferring changes in virulence (10). Phase variation can also occur within an individual strain and as such, *Cj* populations can exhibit phenotypic diversity where some clones remain stable during growth while others do not (43). This intra-strain genetic diversity due to genomic instability is hypothesized to facilitate bacterial survival by conferring a phenotype that allows some clonal cells to survive novel environmental stressors that would prevent growth of the parent cell (44,

45). Thus, the lack of conventional gene regulatory mechanisms could be an alternative strategy for environmental survival between hosts (45).

As mentioned above, *Cj* does possess some known, albeit limited, stress responses important in virulence. The stringent response was shown to be important in virulence-related phenotypes including cell invasion and intracellular survival, as well as for transmission-related phenotypes, as it was shown to be implicated in survival in suboptimal CO_2 or O_2 levels (33). The peroxide-sensing regulator involved in oxidative stress defense, PerR, has also been implicated in pathogenesis mechanisms as *perR* mutations significantly reduced both motility and gut colonization (35).

Cell surface polysaccharides have been shown to participate in transmission and stress survival in *Cj* and therefore are also important pathogenesis factors (6, 34, 46). A large proportion of *Cj*'s small genome is dedicated to enzymes involved in carbohydrate biosynthesis and modification (29). These carbohydrates are incorporated into lipooligosaccharides (LOS), capsular polysaccharides, and *O*-linked flagellar glycoproteins (47, 48), which perform important functions associated with pathogenesis including aiding in *ex vivo* survival, colonization, immune evasion, and serum resistance (6, 47, 49). For instance, purified *Cj* LOS has been implicated in increasing dendritic cell cytokine production as well as in the activation of pro-inflammatory adaptive immune responses (12). Modification of the lipid A component of *Cj* LOS through the addition of amide-linked acyl chains has been shown to provide protection against cationic antimicrobial peptides produced by the innate immune system upon stimulation of TLR-4, as this modification reduces TLR-4 activation (34, 50).

Biofilms are adhered communities of microorganisms encased in a polymeric extracellular matrix (51-53). Most bacterial species exist naturally in sessile biofilms and *Cj* is no exception as

it naturally forms biofilms both *in vitro* and in the environment (54, 55). In biofilms, bacterial cells exhibit altered metabolism and physiology and show an increase in stress tolerance (51). Biofilm formation has been suggested to be a key stress survival factor in *Cj* (54-57), particularly in *ex vivo* survival between hosts (58, 59), as biofilms have been shown to increase *Cj* survival under atmospheric conditions (60, 61) and in water systems (56, 62-65). Biofilm formation is also enhanced in strains lacking stress survival genes like *spoT* (57), mutants with severely truncated LOS chains (66), and in aerobic environments (58), suggesting biofilms are a key survival mechanism in unfavourable conditions.

Autoagglutination, a process whereby cells of the same strain form aggregates, is a known pathogenesis factor in many Gram-negative bacterial pathogens including *Vibrio cholerae* (67), *Bordetella pertussis* (68), and *Neisseria gonorrhoeae* (69), as well as *Yersinia* (70) and *Aeromonas* species (71-73). In *Cj,* strains that demonstrate changes in autoagglutination also show changes in pathogenesis phenotypes. Autoagglutination in *Cj* is known to be associated with cell surface hydrophobicity and other pathogenic factors such as the presence of flagella and the ability to adhere to intestinal cells (29, 74). Pilins (67, 69) and outer membrane proteins (75) have been shown to be autoagglutinins in many bacteria, however specific autoagglutinins have not yet been identified in *Cj*.

Motility is a key pathogenesis factor of *Cj* (76). In order for *Cj* to invade human intestinal epithelial cells and cause disease, it must cross the gastrointestinal mucus, a dynamic gel-like barrier of interlocking glycoproteins that lines these epithelial cells and fills the lumen of intestinal crypts (77, 78). Gastrointestinal mucus is a highly viscous solution; however, *Cj*'s corkscrew-like motility, mediated by its helical shape and polar flagella, allows the cell to move readily through this environment (78-81). In fact, *Cj* exhibits higher velocity moving through viscous media than

through liquid media, which supports the idea that *Cj* is well-suited to the gastrointestinal environment (79). Nonmotile *Cj* mutants are severely impaired in their ability to colonize human or animal host intestinal cells, which further indicates that motility is crucial for colonization and therefore, pathogenesis (78, 82-85). The presence of both motility and flagella are also critical for *Cj* adherence and invasion of epithelial cells (55, 86-88). In addition, flagella are required during biofilm formation to mediate adhesion to other bacteria and to the surface upon which the biofilm is formed (61, 89, 90). Therefore, even though *Cj* flagellin does not stimulate TLR-5 (32), it is still an important pathogenesis factor.

1.4 Morphology as a pathogenesis factor in *C. jejuni*

The overall morphology of a bacterium has biological significance (76, 81). The helical shape of *Cj* has long been identified as a crucial virulence factor as *Cj*'s ability to traverse the gastrointestinal mucus layer utilizing its characteristic corkscrew-like motility is critical for human and zoonotic infection. Direct evidence of the importance of *Cj* morphology in pathogenesis was first provided by our group in 2012 (39), along with a number of key implications for pathogenic properties. Genes and proteins now identified as involved in maintaining cell shape are described below.

Morphology is determined by peptidoglycan (PG), a major component of the bacterial cell wall which, in Gram-negative bacteria, forms a thin layer between the inner and outer cellular membranes (91). PG consists of repeated glycan strands composed of β-1,4 linked *N*-acetylglucosamine and *N*-acetylmuramic acid sugars that are cross-linked by short peptides attached to the *N*-acetylmuramic acid residue (92). In most Gram-negative bacteria, the cross-linkage occurs directly between the amino group, or acyl acceptor, of the side chain at position

three of one peptide subunit (*meso*-diaminopimelic acid in *Cj*), and the carboxyl group, or acyl donor, of the amino acid D-alanine at position four of another peptide subunit (92, 93). The degree of peptide cross-linking within the PG layer can affect the elasticity and permeability of the cell wall (92). PG hydrolases including amidases, endopeptidases, carboxypeptidases, *N*-acetylmuramidases, *N*-acetylglucosaminidases, lysozymes and lytic transglycosylases, are the enzymes responsible for PG modification (94). Almost every PG glycosidic and amide bond can be cleaved by one or more PG hydrolases and as such, many hydrolases play redundant roles (94). Several of these enzymes that have been found in *Cj* are outlined in Appendix A.1 (Figure A.1.1) and will be discussed below. Cell shape, affected by changes in PG structure occurring during PG muropeptide biosynthesis, muropeptide polymerization, or post muropeptide synthesis (80), has long been known to influence physiological and pathogenic phenotypes in bacterial species (95). Modification of the PG layer can also allow for the creation of shapes more complex than rods or spherical cocci, such as the helix (81, 96).

In *Cj*, PG is important for establishing and maintaining its helical morphology. Changes in PG that impact *Cj* morphology have also been shown to affect physiology, colonization, and host-pathogen interactions (39, 45, 77, 97-99). As noted, it was previously hypothesized that *Cj*'s characteristic helical shape conferred a survival advantage over rod-shaped cells (78), since *Cj* shape was until recently only regarded as important for motility (100). The Gaynor lab found that deletion of the PG peptidases *pgp1* or *pgp2* resulted in a rod-shaped morphology that was indeed defective for motility compared to wild type (WT) helical cells but was also defective for biofilm formation and chick colonization (39, 98). The Gaynor lab demonstrated the importance of the overall PG structure in pathogenesis as PG from Δ*pgp1* showed increased activation the human intracellular PG receptor Nod1, whereas PG from Δ*pgp2* showed a decrease in Nod1 activation

compared to WT PG (39, 98). Using a specialized mouse model, the Gaynor lab has also shown that rod-shaped mutants are unable to cross the intestinal mucus layer and cause pathological and inflammatory changes associated with WT *Cj* infection (77). In addition to the phenotypic changes described above, the Gaynor lab also observed a delayed transition to coccoid form in a Δ*pgp1* mutant (99).

Over time, *Cj* populations exhibit a morphological change from helical to coccoid, which occurs not only during the transition to stationary phase (101), but also when cells are subjected to stress via starvation, temperature, pH, osmolarity or oxidation, both on solid, and in liquid, media (54, 99, 102, 103). Recently, the Gaynor lab demonstrated the transition into a coccoid form via PG remodeling by Pgp1 and the amidase AmiA was an important factor in *Cj* virulence properties (99). Indeed, PG from WT coccoid cells reduced activation of human intracellular PG receptors Nod1 and Nod2 compared to PG from helical cells (99). An *amiA* deletion strain not only displayed coccoid formation defects, but also developed a chain-like cell morphology, which highlights the importance of the amidase AmiA (discussed further below) in PG remodelling (99). Hyperosmotic stress has also been shown by the Gaynor lab to induce a chain-like morphology, however the mechanisms behind this transition have yet to be determined (104).

1.5 Peptidoglycan amidases and amidase activators

In order to generate changes in cellular morphology through PG remodelling, PG hydrolases are required (94-96). PG hydrolases cleave bonds in PG or PG fragments, known as muropeptides, for insertion of nascent PG during cell wall growth, PG turnover and recycling, muropeptide release during pathogenesis, and cell lysis (94). However, the most historically well-defined function of PG hydrolases is septal splitting resulting in cell separation during cell division (94). In Gram-negative bacteria, cell division proceeds via the coordinated constriction of the outer

membrane, PG layer, and inner membrane (105, 106). Therefore, PG must be concurrently synthesized and cleaved at the septum to allow separation of the daughter cells while maintaining a complete PG layer (94, 107).

LytC-type *N*-acetylmuramoyl-L-alanine amidases are periplasmic hydrolases that cleave the amide bond between *N*-acetylmuramic acid and the N-terminal amino acid residue of the peptide side chain, L-alanine (107, 108). PG amidases are involved in PG maintenance by hydrolyzing PG but also play a critical role during cell division in the cleavage of septal PG, which allows the release of two daughter cells from the division site (108-110). Along with amidases, lysostaphin-like metalloendopeptidase (LytM) domain-containing proteins are also critical for septal PG cleavage. Indeed, *E. coli* mutants lacking multiple amidases or LytM factors show a severe cell separation defect through the formation of extremely long cell chains connected by fully formed septa that are unable to separate (105, 109-111). Like amidases, LytM factors are widely distributed among bacteria (94, 105, 109, 112, 113). LytM proteins belong to the M23 family of peptidases (peptidase_M23) and many are hypothesized to be putative PG hydrolases involved in important cellular processes like cell elongation and division, cell-shape determination, and sporulation (105, 114-116). Though many characterized LytM domain-containing proteins are metalloendopeptidases able to cleave PG, some LytM proteins show no detectable PG hydrolase activity (117). The most notable and well-studied exceptions are the *E. coli* LytM proteins EnvC and NlpD which appear to have lost metallopeptidase activity (111). However, instead of acting as PG hydrolases, EnvC and NlpD promote cell separation by serving as regulatory factors though activating the *E. coli* amidases.

In regulatory LytM factors, the metalloendopeptidase active site has lost residues involved in PG substrate binding and as a result, can no longer perform PG hydrolysis (117). For instance,

the LytM domains of *E. coli* EnvC and NlpD lack all conserved zinc-chelating and catalytic residues seen in active LytM-like metalloendopeptidases, and instead this domain appears to have adapted to control or enhance PG hydrolysis through interaction with amidases (111, 117-119). It has been demonstrated that although no PG hydrolysis activity was detected in the presence of only EnvC or NlpD, the PG hydrolysis of the *E. coli* amidases AmiA and AmiB was significantly enhanced upon addition of EnvC, and PG hydrolysis by AmiC was significantly enhanced upon addition of NlpD (111). It was also discovered that AmiA, B, and C require direct contact with the LytM proteins for activation to occur (111). In *E. coli,* EnvC was found to be the most critical LytM factor for cell separation, followed closely by NlpD (105).

1.6 LytM proteins as pathogenesis factors

LytM factors have been implicated in pathogenesis mechanisms in several enteric pathogens. In *Salmonella enterica* serovar Typhimurium, EnvC contributes to cell division through the activation of AmiA and AmiC and is also required for intestinal colonization and induction of the inflammatory response in mice (120). In both *S. enterica* and *E. coli*, it has been found that EnvC is critical for resistance to cationic antimicrobial peptides generated by the innate immune response (121). EnvC and NlpD in *V. cholerae* are both involved in cell division by activating its sole amidase AmiB, however only NlpD is required for intestinal colonization in the infant mouse model of cholera (107). In *Pseudomonas aeruginosa* all three LytM proteins work with AmiB in cell division and antibiotic resistance (122).

1.7 *C. jejuni* harbours a putative LytM domain-containing amidase activator

A key enzyme involved in maintaining *Cj* morphology through PG modification is *Cj*'s only PG amidase, AmiA (99). The Δ*amiA* mutant was defective in a helical-to-coccoid

morphology transition and displayed a cell separation defect seen in *E. coli* triple amidase deletion strains where septa were fully formed but cells were unable to separate, thus indicating an important role for AmiA in septum cleavage during cell division (99).

In searching the *Cj* genome for proteins containing peptidase domains, the Gaynor lab identified the *Cj* gene *cjj81176_1291* (hereafter referred to as *1291*, as will all *cjj81176* gene numbers) as a potential factor involved in PG modification. The Gaynor lab also found that deletion of *1291* in *Cj* resulted in a similar morphology to the *amiA* deletion mutant, indicative of a cell separation defect (Chapter 2, E. Frirdich, unpublished data, 99). The *1291* gene product is predicted to be structurally similar to the amidase activators EnvC and NlpD from both *E. coli* and *V. cholerae* (107, 111). As with EnvC and NlpD, 1291 contains an M23 peptidase (LytM) domain that lacks active site residues, which suggests that 1291 also lacks proteolytic activity. Analyses using the free online programs Swiss-Model and HMMER, along with the predicted gene domain structure, have shown that 1291 more closely resembles EnvC than NlpD in *E. coli* and *V. cholerae* (Chapter 3). Furthermore, STRING bioinformatics has predicted that 1291 may interact with AmiA as they show cooccurrence (E. Frirdich & J. Wallace, unpublished data). Together, these data suggest that 1291 may be a homologue of EnvC and/or NlpD, and that 1291 and AmiA may interact via 1291 activation of AmiA.

1.8 Hypothesis

I hypothesize that 1291 is involved in *C. jejuni* morphological changes, and therefore pathogenesis, by activating the PG amidase AmiA.

1.9 Project Aims

My hypothesis will be tested through two aims: the *in vitro* characterization of *C. jejuni 1291* and cross-complementation of *C. jejuni 1291* and *E. coli envC*.

Analysis of cell shape using microscopy and the program CellTool will allow us to assess quantitative morphological differences between the *1291* deletion, complement, and overexpressing strains compared to WT. Additional phenotypic characterization through examination of known *Cj* pathogenesis-related attributes including morphology, motility and biofilm formation will be conducted on the abovementioned *1291* strains in comparison to WT. Assays to be used are standard practice in the Gaynor lab and have revealed clear phenotypic changes compared to WT *Cj* in previously characterized mutants, including those associated with morphological abnormalities and pathogenesis.. The *in vitro* characterization of *1291* will allow us to understand how *1291* and its gene product affect key cellular processes involved in *Cj* biology and disease etiology.

A cross-complementation approach will be undertaken in order to determine if 1291 is required for AmiA activation in *Cj*, similar to how EnvC and NlpD are required for activation of amidases in *E. coli*. Introduction of *1291* into *E. coli* strains lacking *envC* and *nlpD*, and *E. coli envC* into *Cj* Δ*1291*, will allow us to determine if 1291 exhibits activity similar to EnvC and NlpD and to determine if 1291 is a homologue of the *E. coli* amidase activators by observing if there is a reversion to a WT phenotype upon addition of the heterologous gene. This cross-complementation study will allow us to provide insight into if and how 1291 is involved in cell division through activation of AmiA.

1.10 Research Significance

Cj is often the leading cause of food-borne gastroenteritis in developed countries (1), but it is showing increasing resistance to the antibiotics most commonly used in campylobacteriosis treatment: ciprofloxacin and erythromycin (1). Understanding the mechanisms behind *Cj* pathogenesis is still an ongoing process. Studies to further investigate *Cj* virulence mechanisms are hindered by the lack of a reliable disease-susceptible animal model that displays pathology similar to human campylobacteriosis, however this information is crucial to understanding causes and outcomes of *Cj* infection. The most established animal model currently in place is the chick model for *Cj* colonization (82), which does not provide data specific to human *Cj* disease as chicks do not display pathology changes upon infection. Several mouse models have been developed to mimic human *Cj* infection through sensitization of the mouse gastrointestinal tract to *Cj* by genetic modification or depletion of specific gut microbiota (83, 123-128). Though these mouse models have been shown to develop severe gastroenteritis and generate inflammatory immune responses upon infection with *Cj*, these models are all highly specific and relatively new, and their use has not yet been widely adopted. Therefore, *in vitro* analysis of virulence factors is critical to further our current understanding of *Cj* pathogenesis.

Overall, this research will help better understand the contribution of *Cj* cell division and morphology factors in *Cj* pathogenesis. It will also significantly contribute to a growing database of *Cj* shape-determining factors, which can be utilized for the future development of pathogen control strategies including potential targeted antimicrobials.

Chapter 2: *In vitro* characterization of *1291*

2.1 Summary

To understand the importance of *1291* in *C. jejuni* (*Cj*) morphology and pathogenesis, *1291* deletion (Δ*1291*), complement (Δ*1291*c), and overexpressing (*1291*OE) strains were constructed for use in phenotypic assays that have, with mutants previously characterized in our lab, shown clear changes in pathogenesis and morphological phenotypes compared to wild type *Cj* (WT). Deletion of *1291* resulted in a chained, or filamented, morphology, severe motility and autoagglutination deficiencies, a change in cell surface carbohydrates, and an increase in biofilm formation. Complementation at least partially rescued many of the Δ*1291* phenotypic changes and *1291*OE exhibited some phenotypic differences to WT. Therefore, this chapter provides evidence to support the hypothesis that *1291* is involved in cell morphological changes and pathogenesis-associated attributes in *Cj*.

2.2 Materials and Methods

2.2.1 Bacterial growth conditions

All growth conditions are as follows unless otherwise noted.

C. jejuni strains were grown at 38˚C in Mueller-Hinton (MH; Oxoid) broth or on 1.7% (w/v) agar plates supplemented with 5 µg/ml trimethoprim and 10 µg/ml vancomycin (denoted MH-TV), under microaerobic/capnophilic conditions (6% O_2, 12% CO_2) in a Sanyo Tri-Gas incubator for plate cultures, or in a sealed jar containing a CampyGen pack (Thermo Scientific) shaking at 200 rpm for broth cultures. Media were supplemented with 5 µg/ml kanamycin or 2 µg/ml chloramphenicol where appropriate. Stock cultures of strains were frozen at -80˚C in Bacto Brain Heart Infusion (BHI; BD) broth containing 40% glycerol. For use in assays, strains were

pulled from frozen stock cultures onto selective MH-TV plates for overnight growth, followed by 5-6 hr of growth on non-selective MH-TV plates (over-day plates). For further overnight (16-18 hr) growth in broth culture, strains were harvested from over-day plates and diluted to an optical density at 600 nm (OD_{600}) of 0.0005 in MH-TV. Further growth descriptions are provided below for each assay.

E. coli strains were grown at 37˚C in Luria-Bertani (LB; Sigma) broth shaking at 200 rpm, or on 1.5% (w/v) agar plates. Media was supplemented with 5 µg/ml kanamycin or 2 µg/ml chloramphenicol where appropriate. Stock cultures of strains were frozen at -80˚C in LB broth containing 15% glycerol. For use in assays, strains were pulled from frozen stock cultures onto selective LB plates, or into selective LB broth, for overnight growth. Further growth descriptions are provided below for each assay.

2.2.2 Genomic DNA extraction

Cells were resuspended in 600 µl Nuclei Lysis Solution (Promega) and incubated at 80˚C for five minutes. RNaseA (0.02 mg/ml) was added, and the sample was incubated at 37˚C for 30 minutes to one hour. 200 µl Protein Precipitation Solution (Promega) was added, vortexed vigorously to mix and incubated on ice for five minutes to allow for protein precipitation. The sample was centrifuged at 14,000 rpm for three minutes on a Beckman Coulter Microfuge 18 Centrifuge using the 14,000-rpm rotor. The supernatant was transferred to 600 µl isopropanol, inverted to mix and centrifuged at 14,000 rpm for two minutes. The gDNA pellet was washed in 600 µl room temperature (RT) 70% ethanol (EtOH) and centrifuged at 14,000 rpm for two minutes. The supernatant was removed, and the genomic DNA (gDNA) pellet was dried at 42˚C for 10 min.

The gDNA was resuspended in 50 µl nuclease free water, and incubated on ice for at least one hour before storing at -20˚C.

2.2.3 Bacterial strain construction

All bacterial strains and plasmids, and all primers used in this chapter are outlined in Tables 2.1 and 2.2, respectively. All genes cloned into the pRRC plasmid were inserted in the same direction as the *cat* gene and so were expressed under the control of the *cat* promoter (129).

Table 2.1 *C. jejuni* strains, *E. coli* strains, and plasmids used in Chapter 2.

Strains	Genotype or description	Reference or Source
C. jejuni		
81-176	Wild type isolated from a diarrheic patient	(26)
Δ*1291*	81-176 *1291::aphA3*; Km^R	J. Wallace
Δ*1291*c	81-176 Δ*1291 rrn::1291*; Km^R Cm^R	This study
*1291*OE	81-176 *rrn::1291*; Cm^R	This study
Δ*spoT*	81-176 *spoT:: kanR*; Km^R	(33)
Δ*pgp1*	81-176 *pgp1::aphA3*; Km^R	(39)
Δ*amiA*	81-176 *amiA::cat*; Cm^R	(99)
E. coli		
DH5α	F-, φ80d *deoR lacZΔM15 endA1 recA1 hsdR17*(rK-mK+) *supE44 thi-1 gyrA96 relA1 Δ(lacZYA-argF) U169*	Invitrogen
Plasmids		
pGEM-T	PCR cloning vector; Ap^R	Promega
pUC18-K2	Source of non-polar *aphA3* cassette; Ap^R Km^R	(130)
pRRC	*C. jejuni* rRNA spacer integration vector; Cm^R	(129)

Table 2.2 PCR primers used in Chapter 2.

Primer	Sequence (5' to 3')	Restriction Site	Reference
ak233	GCAAGAGTTTTGCTTATGTTAGCAC		(129)
ak234	GAAATGGGCAGAGTGTATTCTCCG		(129)
ak235	GTGCGGATAATGTTGTTTCTG		(129)
ak237	TCCTGAACTCTTCATGTCGATTG		(129)
aphA3-1	CTTATATACCTTAGCAGGAGAC		In house
aphA3-2	CTATTTTTTGACTTACTGGGGA		(39)
cat4	GTGACGGCTTTCATGTTTGC		In house
pRRC-REV1	TAAATGGTGGAGAATAGCGGGAT		In house
1291-L2	GCGTCTAGAGCTCCGTTTTGGTTTAGATC	XbaI	In house
1291-R2	GCACAATTGGCTAAAGCCTCTCCTGAAAA	MfeI	In house
1291-L1	GCTCCGTTTTGGTTTAGATC		In house
1291-R1	GCTGTTGTATCCGTAGTAAAATAAG		In house
1291-IL1	ACGGGTACCGCCTTGAGGGATAGGTAAA	KpnI	In house
1291-IR1	GCGTCTAGATGCCGTAGTGGGTAGAATA	XbaI	In house
1291-LCHK	TGAGAATTTGGCTTTATGAACATA		In house
1291-RCHK	GCATAGCCTCATCATAACTTAAAG		In house

2.2.3.1 *1291* deletion strain construction

The *1291* deletion mutant was constructed by J. Wallace. The *1291* gene was amplified from *Cj* 81-176 gDNA by polymerase chain reaction (PCR) using iProof (Bio-Rad) with 1291-L1 and 1291-R1 primers to yield a 1923 bp product. The product was polyA tailed and ligated to the linear pGEM-T plasmid (Promega). The *1291*_pGEM-T plasmid was transformed into *E. coli* DH5α and inverse PCR was performed on purified *1291*_pGEM-T plasmid with 1291-IL1 and 1291-IL2 primers, deleting 766 bp from the *1291* gene. The inverse PCR product was digested with *KpnI* and *XbaI* (NEB), then ligated to the non-polar kanamycin resistance cassette (*aphA3*) digested from pUC18-K2 (130) using *KpnI* and *XbaI*, creating a Km^R insert in the *1291* gene. The *1291::aphA3* construct was transformed into *E. coli* DH5α and clones were selected by kanamycin resistance. The *1291::aphA3* construct was purified from *E. coli* DH5α using the PureLink HiPure Plasmid Filter MidiPrep Kit (Invitrogen), naturally transformed into *Cj* 81-176 and clones were

selected on kanamycin plates. Genomic DNA was extracted to verify the genotype by iProof PCR analysis and sequencing using the primer pairs 1291-L1/1291-R1 and aphA3-1/aphA3-2. The Δ*1291* strain was reconstructed for Chapter 3 and details regarding its reconstruction can be found in Chapter 3, Section 3.2.2.1.

2.2.3.2 *1291* complement strain construction

The *1291*_pRRC plasmid used in construction of the Δ*1291*c and *1291*OE strains was made by J. Wallace. The *1291* gene including a ribosomal binding site (RBS), and an additional 34 bp upstream of the RBS, was PCR amplified using iProof (Bio-Rad) with 1291-L2 and 1291-R2 primers to yield a 1558 bp product. The PCR product was digested with *XbaI* and *MfeI* (NEB) and ligated into a pRRC plasmid (129) digested using *XbaI* and *MfeI* to create the *1291*_pRRC construct. The construct was transformed into *E. coli* DH5α and selected on chloramphenicol plates. The *1291*_pRRC plasmid was purified using the EZ-10 Spin Column Plasmid DNA Minipreps Kit for Low Copy (BioBasic) to verify construction via iProof PCR analysis and sequencing using the primers cat4, which binds 393 bp upstream of the *1291* gene, and pRRC-REV1, which binds 293 bp downstream of the *1291* gene in the *1291*_pRRC plasmid.

To create the *1291* complement strain, 48 µg of *1291*_pRRC plasmid was purified from *E. coli* DH5α by J. Wallace using the PureLink HiPure Plasmid Filter MidiPrep Kit (Invitrogen). The purified plasmid was naturally transformed into the *1291* deletion strain and selected by kanamycin and chloramphenicol resistance. Genomic DNA was extracted to confirm the genotype via PCR analysis using iProof and sequencing using the primer pairs specified in Section 2.2.3.1 for verification of the native *1291* site, along with cat4/pRRC-REV1 to verify the *1291*_pRRC insert was present, and the forward primers ak233, ak234, and ak235, each with the reverse primer ak237

to determine into which rRNA spacer site the construct was inserted, as the pRRC plasmid can integrate into any of three rRNA spacer regions in *Cj* (129). One copy of the *1291*_pRRC construct was found to have been integrated into the ak234 rRNA spacer site (data not shown).

2.2.3.3 *1291* overexpressing strain construction

To create the *1291* overexpressing strain, 15 µg of *1291*_pRRC plasmid, constructed as described above in Section 2.2.3.2, and purified from *E. coli* DH5α using the PureLink HiPure Plasmid Filter MidiPrep Kit (Invitrogen) was naturally transformed into *Cj* 81-176 and selected by chloramphenicol resistance. Genomic DNA was extracted to confirm the genotype by iProof PCR analysis and sequencing using the primer pairs specified in Section 2.2.3.2 for verification of the *1291*_pRRC insert. One copy of the construct was found to have been integrated into the ak233 rRNA spacer site (data not shown).

2.2.4 Microscopy

2.2.4.1 Slide preparation

Slide preparation is as follows unless otherwise described: 1 µl of broth or plate culture, as described below, was immobilized on a thin 1% agarose (w/v in dH_2O) pad mounted on a glass slide and overlaid with a coverslip.

2.2.4.2 CellTool imaging and image processing

Overnight broth cultures were diluted to an OD_{600} of 0.05 in MH-TV and grown until the OD_{600} was approximately 0.3. Slides were prepared as described above and the cells were imaged by direct interference contrast (DIC) microscopy. Images were captured on a Nikon Eclipse

TE2000-U microscope equipped with a 100X oil immersion objective lens and a Hamamatsu Orca camera system. At least five separate fields of view were imaged to include approximately 300 cells per strain. Image processing was carried out using Adobe Photoshop and ImageJ (National Institute of Health) software. In Photoshop, the image captured on the microscope was converted to 8-bit grayscale. In ImageJ, a radius 1.0 media filter was applied to suppress most of the background noise and the image was converted to binary by adaptive thresholding using the adaptiveThr plugin (https://sites.google.com/site/qingzongtseng/adaptivethreshold). The local threshold was calculated by the mean, using a pixel block size of 102 and subtracting -4. In Photoshop, using the paintbrush tool, artifacts, clumped cells, and partial cells were manually removed. The processed images were analyzed using CellTool software and protocols (131).

2.2.4.3 Membrane staining

For Δ*1291* and WT strains, overnight broth cultures were diluted to an OD_{600} of 0.05 in MH-TV and grown until the OD_{600} was approximately 0.4. FM1-43FX membrane stain (Invitrogen) in DMSO (1 μg/ml) was added and cells were incubated on ice in the dark for 10 min. Since Δ*amiA* does not grow in liquid culture (99), for this study Δ*amiA* was grown on selective MH-TV plates for 48 hr. Δ*amiA* cells were transferred to phosphate-buffered saline (PBS) using an inoculating loop, FM1-43FX membrane stain (1 μg/ml) was added and cells were incubated on ice in the dark for 10 min. All cells were centrifuged at 7,000 rcf for 2 min and resuspended in PBS. Slides were prepared as described above, and cells were imaged using the blue filter for fluorescence microscopy equipped on a Nikon Eclipse TE2000-U microscope. This assay was completed twice for each strain.

2.2.5 Phenotypic analyses

2.2.5.1 Growth curve

The growth curve assay measured both optical density readings and colony forming unit counts. Overnight broth cultures were diluted to an OD_{600} of 0.005 in MH-TV, which also delineates the 0 hour time point. At each time point of 0, 2, 4, 6, 24, 48, and 72 hours, a sample was removed from the culture and used for the OD_{600} measurements, and four serial 10-fold dilutions of the sample were streaked onto MH-TV plates in triplicate and used for CFU/ml counts. After each time point, broth cultures were incubated with a new CampyGen pack, and plates for CFU/ml enumeration were incubated in the Tri-Gas incubator for 48 hours. The CFU/ml was calculated using the dilution that yielded 30-300 colonies per replicate. Statistical significance ($p < 0.05$) for CFU/ml counts was determined for one representative assay using two-way ANOVA, with multiple comparisons. This assay was completed four separate times.

2.2.5.2 Motility

Overnight broth cultures were diluted to an OD_{600} of 0.2 in MH-TV and 2 µl were inoculated into MH-TV plates with 0.4% (w/v) agar. Plates were incubated for 24 hrs, and the halo diameter representing growth of motile cells was measured in mm. If the halo was oblong, the narrowest part of the colony was measured (J. Wallace, personal communication). Plates were imaged using an AlphaImager EC MultiImage Light Cabinet (Alpha Innotech Corporation). Statistical significance ($p < 0.05$) was determined for one representative assay using the pairwise student's t-test. The motility assay was completed three separate times, each with 10 replicate plates.

2.2.5.3 Calcofluor-white assay

Calcofluor-white (CFW) analysis was completed as described previously (57). Overnight broth cultures were diluted to an OD_{600} of 0.2 in MH-TV and 10 µl were spotted in triplicate onto BHI plates containing 1.7% (w/v) agar and 0.002% CFW (fluorescent brightener 28; Sigma) supplemented with 5 µg/ml trimethoprim and 10 µg/ml vancomycin. Plate photos were taken using an iPhoneSE under 365 nm UV light after 24 and 48 hrs of incubation. The CFW assay was completed three separate times with 4 plates, each plate containing three replicates per strain.

2.2.5.4 Biofilm formation

A well-characterized crystal violet assay was used to assess biofilm formation (57, 132). Overnight broth cultures were diluted to an OD_{600} of 0.05 in MH-TV and added to borosilicate tubes. The tubes were incubated standing, without agitation for 24, 48 or 72 hrs. The biofilms were stained using 1% crystal violet (Sigma) in EtOH. After 10 minutes of incubation on the bench at RT, tubes were gently rinsed with cold tap water and allowed to air dry. Biofilms were imaged using an AlphaImager EC MultiImage Light Cabinet (Alpha Innotech Corporation) before dissolution of the crystal violet in destaining solution (10% acetic acid, 30% methanol in dH_2O) for 24 hrs on the bench at RT. Tubes were vortexed vigorously and the absorbance of the dissolved biofilm was measured at 570 nm. Statistical significance ($p < 0.05$) was determined for one representative assay using two-way ANOVA, with multiple comparisons. The biofilm assay was completed four separate times with three replicates per time point.

2.2.5.5 Autoagglutination

The autoagglutination assay was adapted from Misawa and Blaser (74) as follows. Strains were harvested in PBS from non-selective MH-TV plates incubated overnight and diluted to OD_{600} of 1.000. Cell suspensions were allowed to sit undisturbed on the bench at RT for 2, 4, 6, or 24 hrs. At each time point, the top 1 ml of suspension was removed without agitating the suspension, and the OD_{600} was measured. Statistical significance ($p < 0.05$) was determined for one representative assay using two-way ANOVA, with multiple comparisons. The autoagglutination assay was completed three separate times with three replicates per time point.

2.2.5.6 Hydrophobicity

The hydrophobicity assay using hexadecane partitioning was adapted from Rosenberg *et al.* (133) and Ha *et al.* (97). Overnight broth cultures were centrifuged at 6,000 rpm for 10 min at 4˚C in a Beckman Coulter Allegra 25R Centrifuge using a TA-10.250 rotor. The cell pellet was washed in PBS using the same centrifugation conditions for a total of three washes. The cell pellet was resuspended in PBS, diluted to an OD_{600} of approximately 0.5 in PBS, and the initial OD_{600} ($OD_{initial}$) was measured and recorded. A ratio of 1:4 hexadecane (Sigma) to culture by volume was added and vortexed vigorously for 5 min to mix. Cell suspensions were incubated at 37˚C for 30 min to allow the hydrophobic and aqueous layers to separate. The aqueous layer was removed and left open to the air for 10 min to ensure evaporation of any hexadecane, and the final OD_{600} (OD_{final}) was measured. The percent hydrophobicity was determined by the calculation below. Statistical significance ($p < 0.05$) was determined for one representative assay using the unpaired student's t-test. The hydrophobicity assay was completed three separate times with three replicates per strain.

$$\frac{OD_{(initial)}-OD_{(final)}}{OD_{(initial)}} \times 100\% = \%\ \text{hydrophobicity}$$

2.3 Results

2.3.1 Deletion of *1291* alters *C. jejuni* cell shape

To visually observe overall cell morphology, DIC microscopy images were taken. At least five images per strain were analyzed with Figure 2.1 showing a representative field of view. The WT, Δ*1291*c and *1291*OE strains appeared to have similar cellular morphology whereas the deletion of *1291* caused a significant change in cell shape (Figure 2.1). The long chained, or filamented, phenotype exhibited by Δ*1291* was also observed with the Δ*amiA* deletion strain (Figure 2.1, 99). The Δ*1291*c strain appeared to yield full shape complementation compared to Δ*1291*c and WT (Figure 2.1).

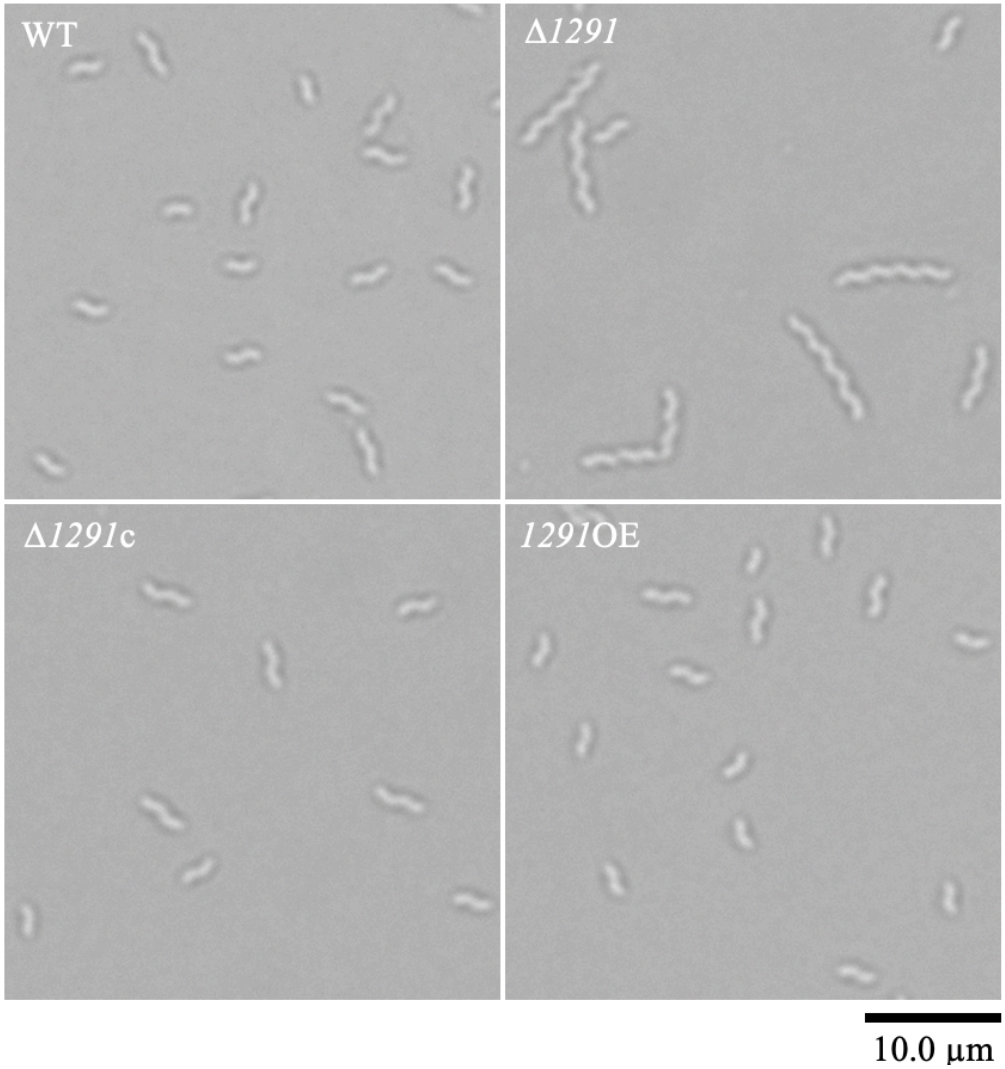

Figure 2.1 Cellular morphology of WT, Δ*1291*, Δ*1291*c, and *1291*OE strains. Strains were imaged by DIC microscopy at 100X magnification.

To quantify the cellular morphology changes of each of the *1291* strains compared to WT, CellTool software was utilized (131). A wild type model was generated from approximately 300 wild type cells over at least five fields of view imaged by DIC microscopy (Figure 2.2).

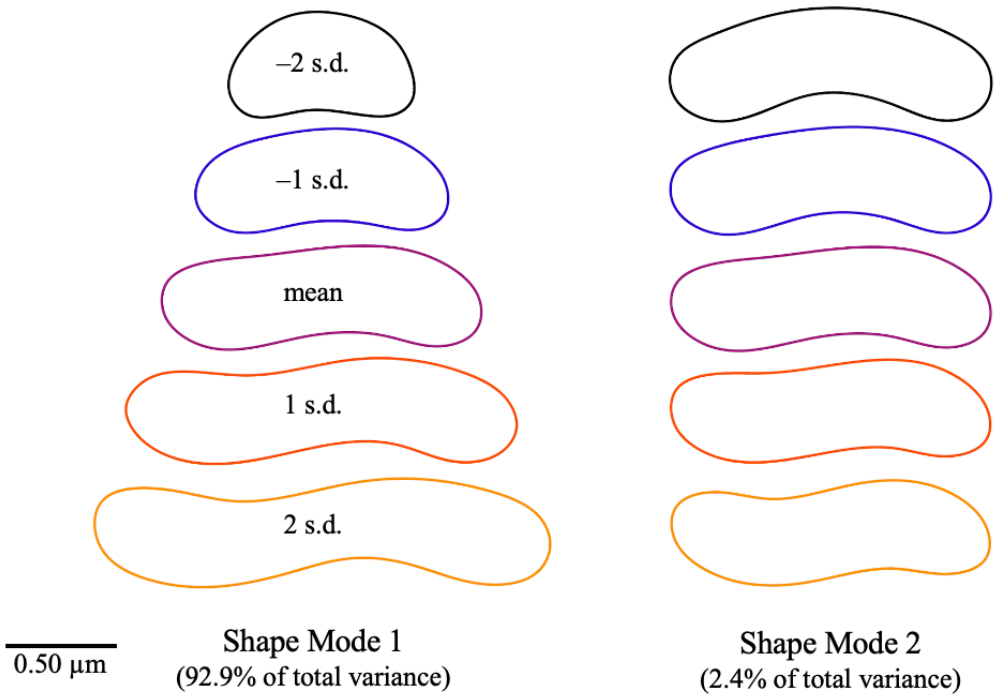

Figure 2.2 CellTool wild type model. The WT model was generated from principal component analysis of approximately 300 *Cj* WT cells. Two shape modes describe 95.3% of variance between the WT cells. Shape Mode 1, which accounts for 92.9% of total variance, describes length, and Shape Mode 2, which accounts for 2.4% of total variance, describes helical pitch. The mean of the wild type model is denoted in purple while the other colours indicate standard deviations (s.d.) from the mean.

Two shape modes were determined to account for 95.3% of the total variance, which were length (described by Shape Mode 1, accounting for 92.9% of variance) and helical pitch (described by Shape Mode 2, accounting for 2.4% of variance) (Figure 2.2, Figure 2.3). The wild type model was compared to measurements generated from approximately 300 cells of each of the other strains (Δ*1291*, Δ*1291*c, and *1291*OE) to generate models comparing cell length and helical pitch.

For Shape Mode 1, negative and positive standard deviation from the mean indicate shorter and longer cells, respectively. The Δ*1291* cells were the longest due to the high positive standard deviation from the mean and had much more variation in length compared to the other strains as the relative abundance of cells was spread over a wide range of standard deviations from the mean

(Figure 2.3A). The Shape Mode 1 distribution also showed that cells from the Δ*1291*c strain were slightly longer than WT and *1291*OE cells (Figure 2.3A), which was unclear from the DIC image data (Figure 2.1). Nonetheless, it is clear that Δ*1291*c showed a considerable degree of phenotypic complementation compared to Δ*1291*.

In Shape Mode 2, negative and positive standard deviation from the mean indicate a lower degree of helical pitch (i.e., a compressed helix or a more defined kink), and a higher degree of helical pitch (i.e., a stretched helix or a flatter curve), respectively. WT, Δ*1291*c, and *1291*OE cells all had a similar helical pitch, while Δ*1291* cells showed more variation in helical pitch and had a much more defined curvature compared to WT (Figure 2.3B). Although most Δ*1291* cells exhibited helical pitch within -5 standard deviations from the mean, some displayed a degree of helical pitch upwards of -50 standard deviations from the mean (Figure 2.3B). Though Δ*1291*c showed notable, albeit incomplete, complementation of length compared to Δ*1291* and WT (Figure 2.3A), Δ*1291*c appeared to show full complementation of helical pitch (Figure 2.3B).

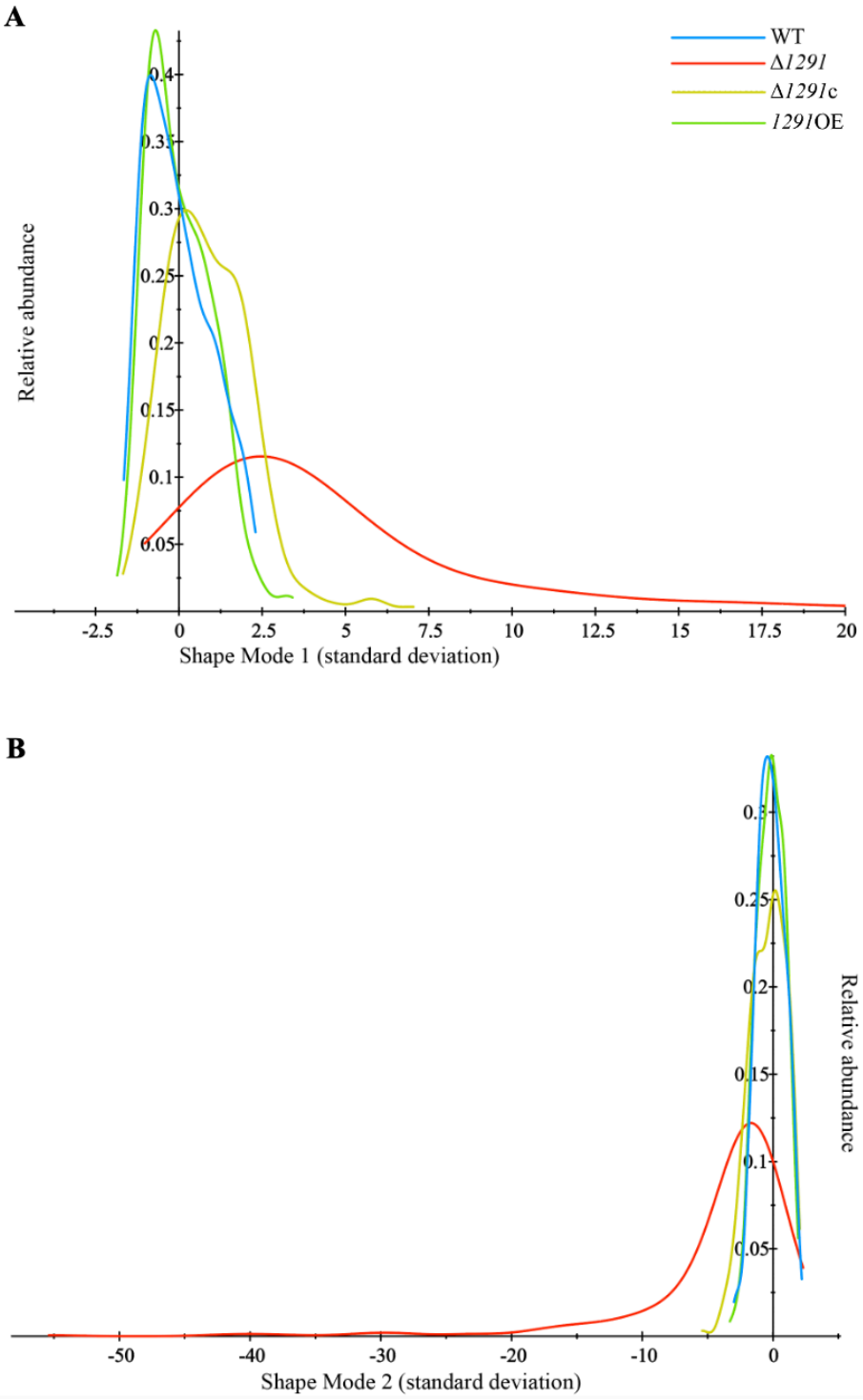

Figure 2.3 Distribution and relative abundance for length and helical pitch of the *1291* strains compared to WT. A) Shape Mode 1 (length), and B) Shape Mode 2 (helical pitch). The models were generated using CellTool by comparing approximately 300 cells from each strain to the wild type model shown in Figure 2.2. WT (blue), Δ*1291* (red), Δ*1291*c (yellow), and *1291*OE (green).

To determine if Δ*1291* was indeed chained (multiple cells unable to separate) or filamented (one elongated cell), the membrane was stained using the membrane dye FM1-43FX. Initial attempts to observe septa were inconclusive due to background fluorescence, so the protocol underwent optimization. Cells were fixed in 2.5% formaldehyde in PBS and mounted on 0.1% poly-L-lysine (Sigma) coated coverslips (data not shown), however cells were most easy to focus when live-mounted on agarose gel pads, and thus images in Figure 2.4 were obtained using this method. The known chained mutant lacking the amidase AmiA (Δ*amiA*) was used as a control (99), but the results were inconclusive. I was unable to clearly discern septa in the long Δ*1291* chain-like cells, however some Δ*1291* and Δ*amiA* cell chains appeared to have septa (Figure 2.4). Overall, only a few Δ*1291* and Δ*amiA* cell chains displayed putative septa, so the membrane staining results were promising but inconclusive as to whether Δ*1291* exhibited a chained or filamented morphology.

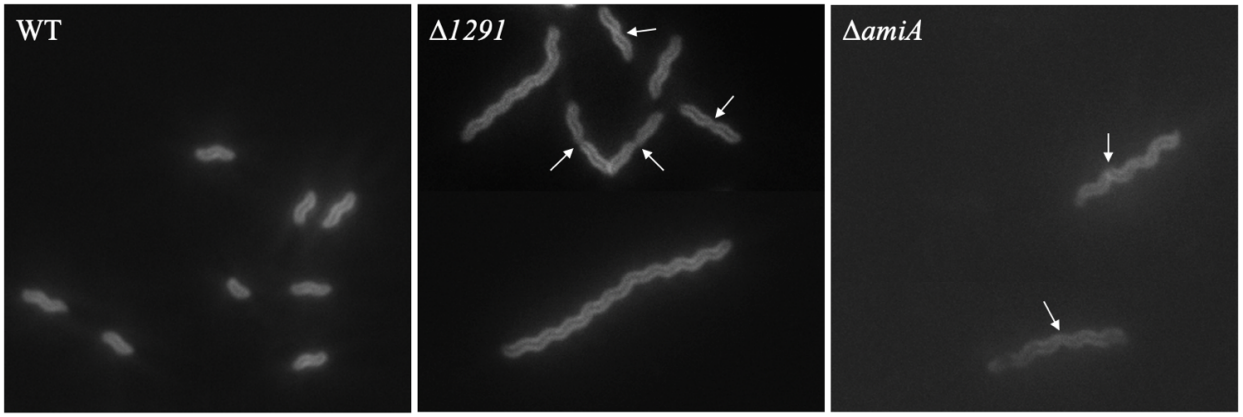

Figure 2.4 Cell morphology of WT, Δ*1291*, and Δ*amiA* strains as visualized by FM1-43FX membrane stain. Cells were stained with 1 µg/ml FM1-43FX in DMSO and live mounted on agarose gel pads. Images were captured at 100X magnification using a blue fluorescence filter. Arrows indicate putative septa.

2.3.2 All *1291* strains show some growth impairment compared to wild type

The growth curve assay included both optical density readings of each culture, as well as colony forming unit counts at each time point. Each separate assay showed the same trend for the OD_{600} readings: *1291*OE had impaired growth during log phase compared to all other strains, as demonstrated by the lowest OD_{600} reading at 24 hours, and Δ*1291*, Δ*1291*c, and *1291*OE all had lower OD_{600} readings than WT in stationary phase (Figure 2.5A). Despite having an OD_{600} similar to WT between 0 and 24 hours (Figure 2.5A), Δ*1291* had the fewest CFU/ml of all strains, which was statistically significant compared to WT (Figure 2.5B). The disconnect between the optical density reading and the CFU/ml count may be due to the elongated shape of the mutant distorting the optical density reading. Therefore, it is tempting to hypothesize that one long cell corresponds to one colony forming unit. Previously in our lab, a decrease in CFU/ml has been correlated with an increase in the degree of filamentation however, this correlation has yet to be confirmed (104).

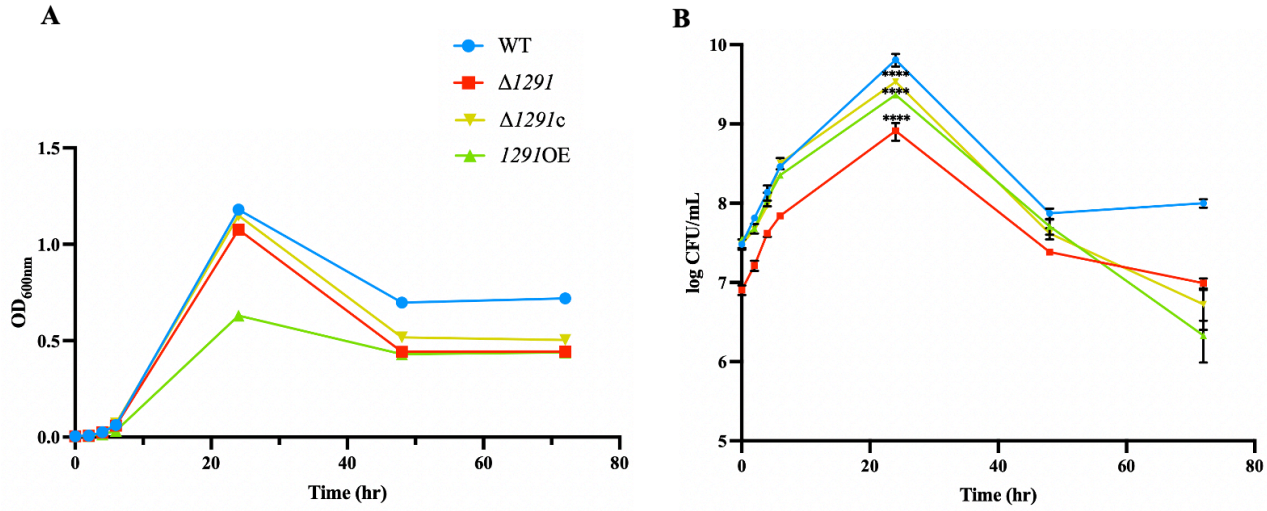

Figure 2.5 Growth curve analysis of WT, Δ*1291*, Δ*1291*c, and *1291*OE strains grown in broth. A) Optical density measurements at 600nm (OD_{600}) for one replicate per strain, and B) colony forming unit counts per ml were obtained after 0, 2, 4, 6, 24, 48, and 72 hrs. Four 10-fold serial dilutions were streaked in triplicate for quantifying CFU/ml. The CFU/ml was calculated using the dilution that yielded 30-300 colonies per replicate. The asterisk (*) indicates a statistically significant difference compared to WT determined by the two-way ANOVA test with multiple comparisons, with **** indicating $p < 0.0001$. Error bars show standard deviation. WT (blue), Δ*1291* (red), Δ*1291*c (yellow), and *1291*OE (green).

2.3.3 Loss of *1291* affects motility, CFW reactivity, biofilm formation and autoagglutination

The motility assay showed that Δ*1291* had a severe, and statistically significant, motility defect compared to wild type (Figure 2.6). The severe motility impairment due to deletion of *1291* is likely in part due to its elongated shape, as it has been previously observed by the Gaynor lab via transmission electron microscopy that Δ*1291* has intact flagella (E. Frirdich & J. Wallace, unpublished data). The complement showed incomplete but statistically significant complementation compared to Δ*1291*, while *1291*OE had similar motility to WT (Figure 2.6).

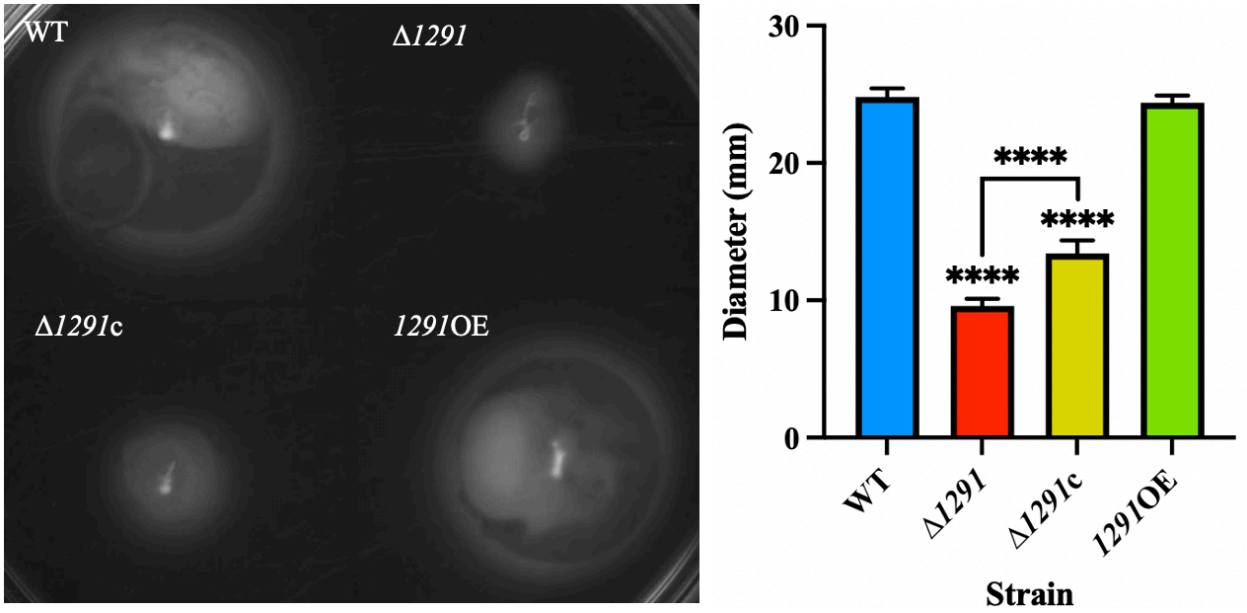

Figure 2.6 Motility of WT, Δ*1291*, Δ*1291*c, and *1291*OE strains. Motility was assayed on 10 replicate 0.4% agar plates by measuring the diameter of the halo formed around the central inoculation site after 24 hrs incubation. The asterisk (*) indicates a statistically significant difference compared to WT (above the bars) or between Δ*1291* and Δ*1291*c (above the bracket) determined by the pairwise student's t-test with ****, indicating $p < 0.0001$. Error bars show standard deviation.

Previously in the Gaynor lab, it was shown that mutants displaying altered CFW reactivity compared to WT also showed changes in stress survival and pathogenesis phenotypes (39, 45, 57, 66, 98). In addition to WT, the *1291* strains were compared to the hypofluorescent (dim) straight mutant strain, Δ*pgp1*, and the hyperfluorescent (bright) stringent response deletion mutant strain, Δ*spoT*. After 24 hours, Δ*1291* showed similar fluorescence to Δ*spoT*, while the fluorescence of WT, Δ*1291*c, and *1291*OE were similar to the dim strain Δ*pgp1* (Figure 2.7). At 48 hours, Δ*1291* exhibited fluorescence similar to Δ*1291*c, which was between the bright Δ*spoT* strain and WT (Figure 2.7).

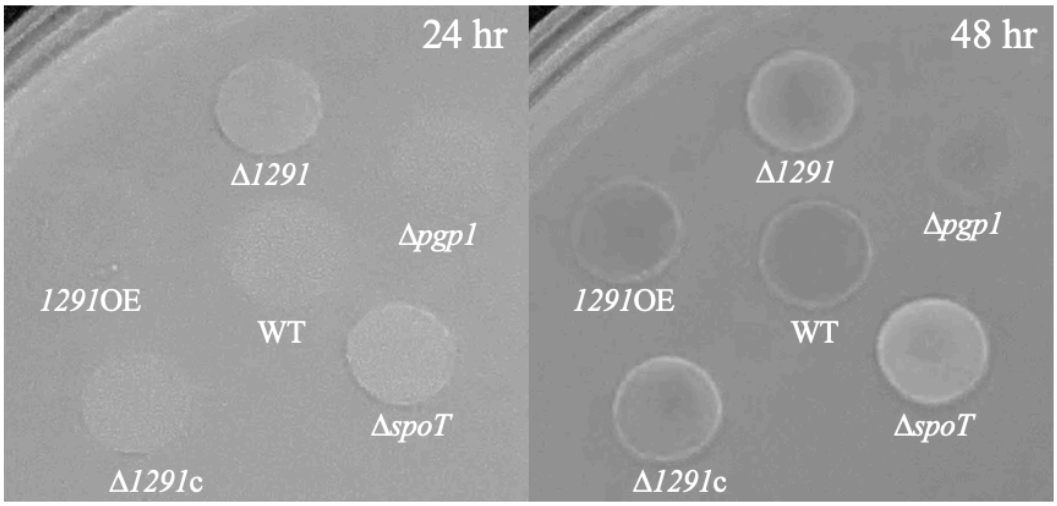

Figure 2.7 Calcofluor-white reactivity of WT, Δ*1291*, Δ*1291*c, and *1291*OE strains spotted onto BHI plates containing 0.002% CFW. Representative CFW reactivity from 12 replicates is shown. Plates were imaged after 24 and 48 hrs incubation under 365 nm UV light. The control strains used were the hypofluorescent straight mutant strain, Δ*pgp1*, and the hyperfluorescent stringent response mutant strain, Δ*spoT*.

When looking at the formation of biofilms in each of the *1291* strains, the biofilm grew both at the air-liquid interface of the media in the glass tubes, as well as on the bottom of the tube, which has been seen frequently in our lab (57) (Figure 2.8A). Δ*1291*c fully rescued the rapid biofilm formation shown by Δ*1291* at 24 and 48 hours but had significantly less biofilm formation at 72 hours compared to WT (Figure 2.8B). Biofilm levels were more comparable after three days for WT, Δ*1291* and *1291*OE (Figure 2.8B).

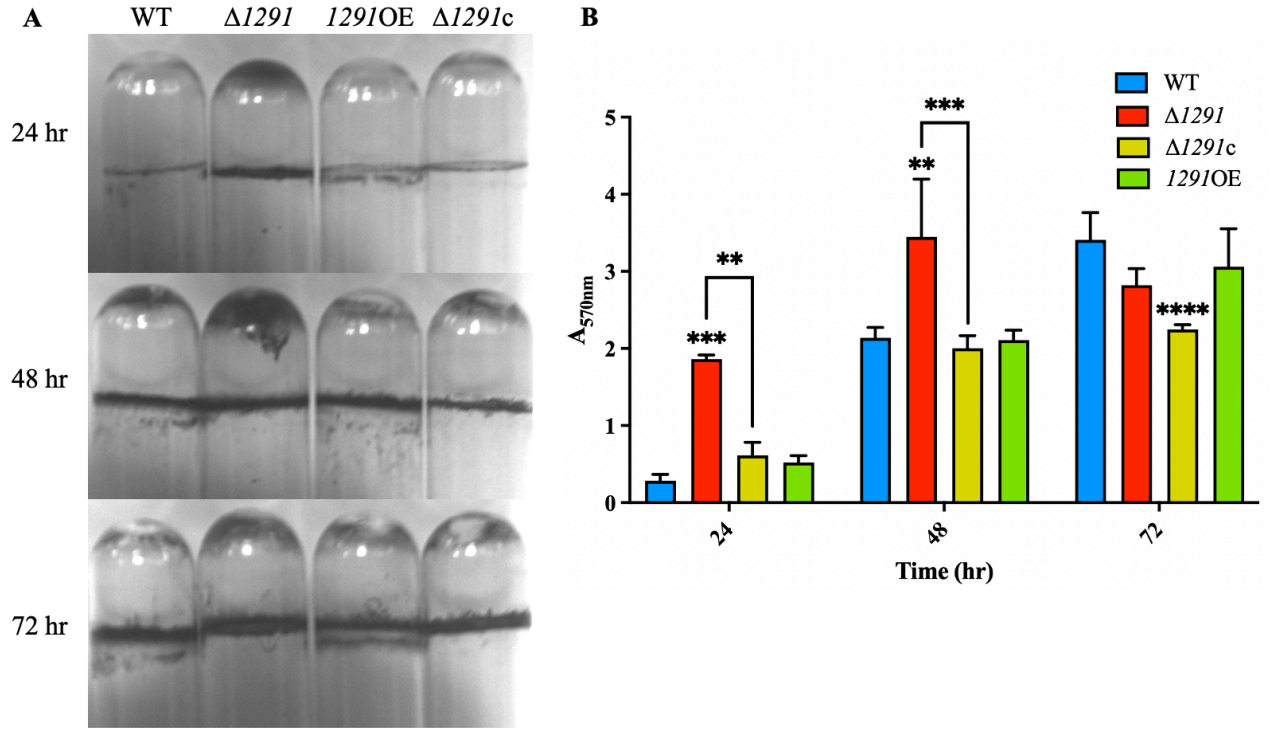

Figure 2.8 Biofilm formation of WT, Δ*1291*, Δ*1291*c, and *1291*OE. Biofilms were grown on borosilicate glass tubes for 24, 48 and 72 hrs, and stained with crystal violet. A) The biofilm formation was imaged for one representative tube of three replicates before the crystal violet was dissolved and B) the absorbance at 570 nm (A_{570nm}) was measured for all three replicates. The asterisk (*) indicates a statistically significant difference compared to WT (above the bars) or between Δ*1291* and Δ*1291*c (above the brackets) determined by the two-way ANOVA test with multiple comparisons, with **, ***, and ****, indicating $p < 0.01$, $p < 0.001$, and $p < 0.0001$, respectively. Error bars show standard deviation.

The rate of autoagglutination in PBS of each strain was determined by measuring the OD_{600} of the top 1 ml of cell suspension after undisturbed incubation on the benchtop. Δ*1291* had a statistically significant autoagglutination defect compared to WT (Figure 2.9). The Δ*1291*c strain showed no complementation in this assay compared to Δ*1291* (Figure 2.9). One possible explanation for this result is that the elongated shape of Δ*1291* does not contribute to the severe loss of autoagglutination for this strain.

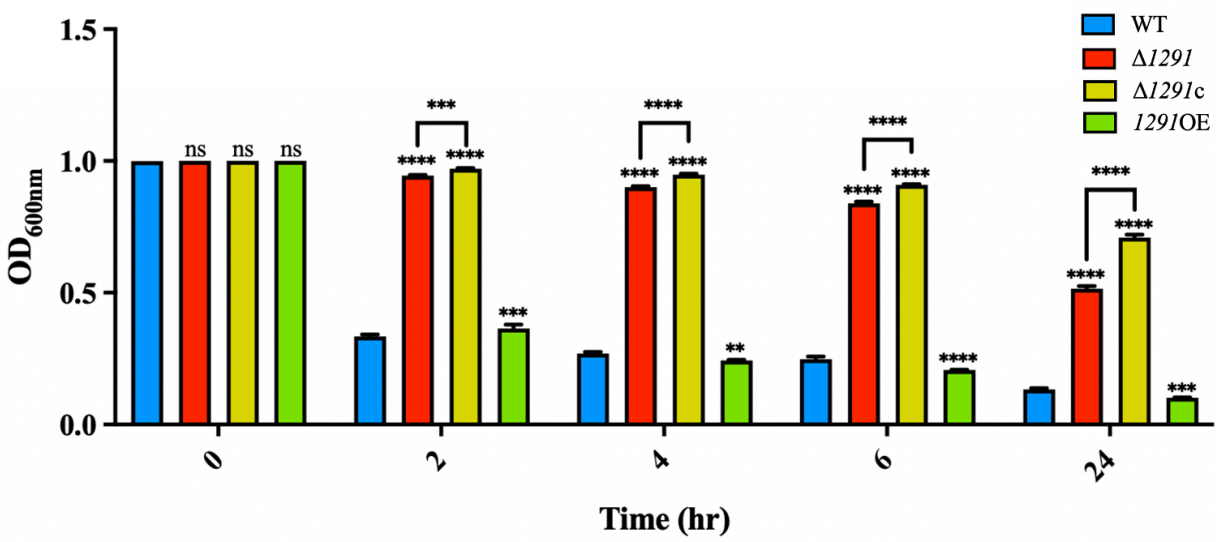

Figure 2.9 Autoagglutination of WT, Δ*1291*, Δ*1291*c, and *1291*OE in PBS. Cells were suspended undisturbed in PBS for 2, 4, 6 or 24 hrs. The OD_{600} readings were taken from the top 1 ml of the PBS suspension at each time point for each of three replicates. The asterisk (*) indicates a statistically significant difference compared to WT (above the bars) or between Δ*1291* and Δ*1291*c (above the brackets) determined by the two-way ANOVA test with multiple comparisons, with **, ***, and ****, indicating $p < 0.01$, $p < 0.001$, and $p < 0.0001$, respectively (ns = non-significant). Error bars show standard deviation. WT (blue), Δ*1291* (red), Δ*1291*c (yellow), and *1291*OE (green).

The hydrophobicity of each strain was assayed using hexadecane partitioning, which had been used previously in our lab for one project (97); however, it is not standard practice in our lab. Hexadecane was added to cell suspension in PBS and, after thoroughly vortexing, the hydrophobic (hexadecane) and aqueous (PBS) layers were allowed to separate before the OD_{600} of the aqueous layer was measured. In all cases except for *1291*OE, the OD_{600} of the aqueous layer after the incubation period had increased compared to the initial OD_{600} measured before the hexadecane was added, thus resulting in a negative percent hydrophobicity (Figure 2.10). The negative percent hydrophobicity result was seen over multiple separate experiments and had not been seen when this assay was completed previously in our lab (Ha et al 2016). A literature search after several assay attempts confirmed that this method is not useful for measuring hydrophobicity in *Cj* (134).

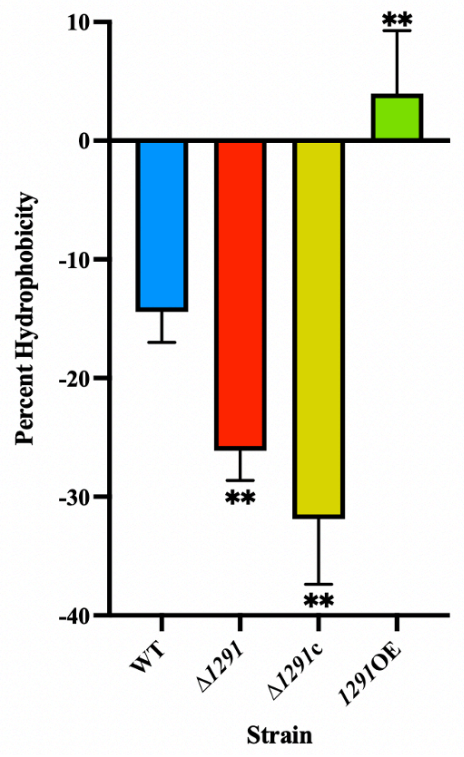

Figure 2.10 Percent hydrophobicity of WT, Δ*1291*, Δ*1291*c, and *1291*OE measured by hexadecane partitioning. Hexadecane was added to cell suspensions in PBS and mixed thoroughly. The OD_{600} of the aqueous layer was measured for each of three replicates after the aqueous and hydrophobic layers were allowed to separate and the % hydrophobicity was calculated. The asterisk (*) indicates a statistically significant difference compared to WT determined by the unpaired student's t-test with ** indicating $p < 0.01$. Error bars show standard deviation.

2.4 Discussion

In this study, the cellular morphology and pathogenesis phenotypes of *Cj 1291* were characterized. The deletion of *1291* resulted in a long chain-like phenotype which resembled the previously observed Δ*amiA* phenotype (99). However, as Δ*amiA* cannot be grown in liquid culture (99), only the cellular morphology and motility of Δ*1291* could be directly compared to *Cj* Δ*amiA* phenotypes, which are discussed further below.

The Δ*1291*c and *1291*OE strains were constructed using the *1291*_pRRC plasmid, which in each strain, integrated into one of three rRNA spacer regions in the *Cj* genome. Genes expressed

in pRRC are under control of the reasonably strong non-native *cat* promoter, rather than the native *Cj* promoter (129). Previously in our lab, it was shown that higher than optimal expression of the PG peptidase gene *pgp1* by the *cat* promoter resulted in a lack of phenotypic complementation (39). Therefore, non-native expression from the pRRC *cat* promoter resulting in a lower than optimal expression of *1291* could account for the lack of complementation by Δ*1291*c in the autoagglutination assay, since the overexpression of *1291* did not result in a loss of autoagglutination compared to WT (Figure 2.9). The non-native *1291* expression in Δ*1291*c may also be the cause of incomplete complementation observed in the growth curve, motility, and biofilm formation assays (Figures 2.5, 2.6, and 2.8).

The FM1-43FX membrane stain has demonstrated clear cell chaining phenotypes in *E. coli* mutants lacking amidases and amidase-activators (Chapter 3, 105, 111), but our results suggest that *Cj* may be too small for the membrane stain to consistently penetrate the septa. Putative septa were observed in some of the short Δ*1291* chain-like cells and in the known chained Δ*amiA* mutant, however no clear septa could be visualized in the longer Δ*1291* chain-like cells (Figure 2.4, 99). The Gaynor Lab has also had difficulties in the past with membrane dyes and fluorescent molecules unable to penetrate the *Cj* membrane due to the small size of *Cj* (E. Frirdich and J. Wallace, personal communication). Thus, although the FM1-43FX membrane stain can be used as a method to visualize the overall shape of *Cj* and observe septa in *E. coli* (Chapter 3, 105, 111), it is not an effective method to clearly distinguish between chained and filamented cell morphology phenotypes in *Cj*.

All *1291* strains exhibited some growth impairment compared to WT, with *1291*OE showing the lowest OD_{600} reading at 24 hours (Figure 2.5). In *E. coli*, a truncated version of EnvC containing only the LytM domain demonstrated severe toxicity as cell lysis was triggered even at

low level induction (111). Therefore, the impaired growth rate of *1291*OE may be due to the increased amount of 1291 protein expression slightly increasing its toxicity enough to decrease growth rate but not affect overall survival.

Despite its chain-like phenotype, the Δ*1291* strain retained some, albeit significantly impaired, motility which was likely due to its intact flagella (Figure 2.6, E. Frirdich and J. Wallace, unpublished). The chained *Cj* Δ*amiA* mutant lacked flagella and thus was nonmotile (99), but in another helical bacteria, *Helicobacter pylori*, the chained Δ*amiA* deletion mutant lacked motility despite possessing intact flagella (135). The *Cj* mutant Δ*pgp2*, which did not demonstrate any flagellar defects but had a straight cellular morphology, also showed reduced motility compared to WT (98), confirming that both intact flagella and shape are important in motility. Motility has also been shown to aid in the kinetics of biofilm formation in *Cj* (55, 58, 90) but the severe motility defect of Δ*1291* did not hamper its biofilm formation as this was likely mediated by the presence of intact flagella, a known adhesin in biofilm formation (55, 61, 89, 90).

CFW binds to β-1,3 and β-1,4 carbohydrate linkages and fluoresces under 365 nm UV light (57, 136). Therefore, it is reasoned that differences in CFW reactivity likely reflect differences in surface carbohydrate composition. In *Salmonella enteritidis*, *S. enterica*, and *E. coli*, CFW binds extracellular cellulose which has been shown to be important in biofilm formation (137-139). The exact carbohydrates that vary in *Cj* due to increased or decreased CFW reactivity are unknown, as we have thus far been unable to link CFW reactivity differences to specific changes in well-characterized *Cj* surface sugars (i.e., LOS, and capsule or *N*-linked polysaccharides) (57). In this study, the CFW hyper-reactive mutant Δ*1291* formed biofilms much more rapidly than WT, Δ*1291*c and *1291*OE (Figure 2.8B; 24 and 48 hour timepoints), which correlates with previous

observations in our lab that CFW hyper-reactive strains overproduce biofilms, while hypo-reactive mutants are defective in biofilm formation (39, 57).

Generally, mutants that show an increase in biofilm formation also show an increase in autoagglutination as they share many of the same mechanisms including hydrophobicity and carbohydrate binding (58, 74, 140). Carbohydrate changes in certain known surface moieties have been shown to correlate with biofilm formation in *Cj* – i.e., the LOS (66) and outer membrane proteins (141). The altered CFW reactivity of Δ*1291* compared to WT demonstrated that there are cell surface carbohydrate changes that occur upon deletion of *1291*. Indeed, CFW-reactive polysaccharides have been linked to biofilm formation in *P. aeruginosa* and *S. enteritidis* (137, 142). Therefore, the conflicting biofilm formation and autoagglutination results may be due to changes in cell surface carbohydrates that benefit biofilm formation but not autoagglutination in solution. Autoagglutination has also been associated with the presence of intact flagella, as aflagellate mutants showed severe autoagglutination defects (74). Δ*1291* possesses intact flagella however, which suggests the autoagglutination defect could be due to changes in its cell surface.

In *E. coli*, *S. enterica*, and *P. aeruginosa*, defects in septal cleavage have been found to be detrimental to cell membrane integrity and increase cellular envelope stress (121, 122, 143). For instance, severely chained *E. coli* mutants lacking all three amidases, showed sensitivity to detergents and high molecular weight antibiotics as did amidase deficient *P. aeruginosa* strains (122, 143). In addition, *S. enterica* strains developed sensitivity to cationic antimicrobial peptides upon deletion of *envC* (121). Therefore, the lower helical pitch, or more compressed helix, in Δ*1291* cells may be due to high cellular envelope stress arising from their elongated morphology (Figure 2.3B). Alternately, the helical pitch of Δ*1291* could be the cause of increased envelope stress. Envelope stress was recently shown to be a factor in the initiation of biofilm formation in

Cj (55). Under stressful conditions, *Cj* strains have been shown to adapt to the biofilm lifestyle more quickly than under optimal growth conditions, with biofilms formed under each condition reaching similar levels after three days (58) as was seen in this study (Figure 2.8B). Though shown to be expendable for primary biofilm attachment, extracellular DNA (eDNA), released via autolysis (144, 145) has been shown to significantly contribute to biofilm structure and function in *Cj* (55, 144, 146). It is likely that Δ*1291* experiences some envelope stress as indicated by the lower helical pitch compared to the much more relaxed helix of the WT strain (Figure 2.3B). As such, the rapid biofilm formation shown by Δ*1291* (Figure 2.8) could at least in part be due to a decrease in cell membrane integrity leading to increased eDNA release via an increase in membrane permeability or cell lysis.

Further studies will be needed to elucidate the mechanisms underlying the Δ*1291* phenotypes. However, as Δ*1291* showed clear changes in both morphology and pathogenesis phenotypes compared to WT, *1291* can be described as an important shape determinant and pathogenesis factor in *Cj*.

Chapter 3: Cross-complementation of *C. jejuni 1291* and *E. coli envC*

3.1 Summary

In order to determine if 1291 functions as an amidase activator, *Cj 1291* was cross-complemented into *E. coli* amidase activator deficient strains, and *E. coli envC* was cross-complemented into *Cj* Δ*1291*. A version of *1291* that was codon-optimized for expression in *E. coli* (*1291CO*) was synthesized and used in this study. The addition of *1291CO* to the double amidase activator deficient strain *E. coli* Δ*envC*Δ*nlpD*, and *envC* to Δ*1291* resulted in a partial, though clear, reversion to the respective wild type phenotypes. As 1291 and EnvC appeared to be able to stimulate amidases across species, this chapter provides evidence towards the hypothesis that 1291 is involved in amidase activation.

3.2 Materials and methods

3.2.1 Bacterial growth conditions

Bacterial growth conditions are as stated in Chapter 2, Section 2.2.1.

3.2.2 Bacterial strain construction

All bacterial strains and plasmids, and all primers used in this chapter are outlined in Tables 3.1 and 3.2, respectively. The pRRC plasmid is integrative in *C. jejuni* as described previously (Chapter 2, Section 2.2.3.2), but is replicative in *E. coli* (129). All genes cloned into the pRRC plasmid were inserted in the same direction as the *cat* gene and so were expressed under the control of the *cat* promoter (129).

Table 3.1 *C. jejuni* strains, *E. coli* strains, and plasmids used in Chapter 3.

Strains	Genotype or description	Reference or Source
C. jejuni		
81-176	Wild type isolated from a diarrheic patient	(26)
Δ*1291*	81-176 *1291::aphA3*; Km^R	Reconstructed for this study
Δ*1291* + (*envC*_pRRC)	81-176 Δ*1291 rrn::envC* (*envC* from TB28); Km^R Cm^R	This study
E. coli		
DH5α	F-, φ80d *deoR lacZΔM15 endA1 recA1 hsdR17*(rK-mK+) *supE44 thi-1 gyrA96 relA1 Δ(lacZYA-argF) U169*	Invitrogen
TB28	*rph1 ilvG rfb-50 ΔlacIZYA::frt*	(105)
Δ*envC*	TB28 *ΔenvC725::*Km^R (TB134)	(105)
Δ*nlpD*	TB28 Δ*nlpD747::*Km^R (TB139)	(105)
Δ*envC*Δ*nlpD*	TB28 *ΔenvC725::frt* Δ*nlpD747::*Km^R (TB156)	(105)
Δ*envC* + (*1291CO*_pRRC)	TB28 *ΔenvC725::*Km^R expressing codon-optimized *1291*; Km^R Cm^R	This study
Δ*nlpD* + (*1291CO*_pRRC)	TB28 Δ*nlpD747::*Km^R expressing codon-optimized *1291*; Km^R Cm^R	This study
Δ*envC*Δ*nlpD* + (*1291CO*_pRRC)	TB28 *ΔenvC725::frt* Δ*nlpD747::*Km^R expressing codon-optimized *1291*; Km^R Cm^R	This study
Plasmids		
pRRC	*C. jejuni* rRNA spacer integration vector; Cm^R	(129)

Table 3.2 PCR primers used in Chapter 3.

Primer	Sequence (5' to 3')	Restriction Site	Reference
ak233	GCAAGAGTTTTGCTTATGTTAGCAC		(129)
ak234	GAAATGGGCAGAGTGTATTCTCCG		(129)
ak235	GTGCGGATAATGTTGTTTCTG		(129)
ak237	TCCTGAACTCTTCATGTCGATTG		(129)
cat4	GTGACGGCTTTCATGTTTGC		In house
pRRC-REV1	TAAATGGTGGAGAATAGCGGGAT		In house
1291CO-L2	GCTATCTAGAGTCCTCGGTCCTGGTATG	XbaI	This study
1291CO-R2	GCACAATTGCAAGGGCTTCTCCGGAA	MfeI	This study
1291CO-mid	GAAGTTCATACCAAGGGTCGA		This study
EnvC-F	GCTATCTAGAGAGGGGAAAGGCGATTAATACC	XbaI	This study; Modified from Uehara *et al*. (105)
EnvC-R	CCGGAATTCCGGGAGCGGCAAATGCAAGAACG	EcoRI	This study; Modified from Uehara *et al*. (105)
EnvC-mid	GCAACAAACGCTGTTATATGAGCAG		This study

3.2.2.1 Reconstruction of the *1291* deletion strain

Over time, and multiple freeze/thaw cycles, the growth of *Cj* strains can slow down and, in some cases, cease as was seen with a Δ*amiA* strain previously (99). Therefore, it is common to have to remake *Cj* strains to ensure fidelity (E. Gaynor, personal communication, 99). Genomic DNA was extracted from the Δ*1291* strain used in Chapter 2 as described previously (Chapter 2, Section 2.2.2), and naturally transformed into *Cj* 81-176. Transformants were selected on kanamycin plates and gDNA was extracted to confirm the genotype by iProof PCR analysis using the primer pairs aphA3-1/1291-LCHK and aphA3-2/1291-RCHK.

3.2.2.2 Electrocompetent *E. coli* strain preparation

E. coli strains Δ*envC*, Δ*nlpD*, and Δ*envC*Δ*nlpD* were made to be electrocompetent. Overnight broth cultures were diluted 1/50 in LB broth and grown to an OD_{600} of approximately 0.5. Cultures were incubated on ice for 10 min and centrifuged at 8,000 rpm for 5 min at 4˚C in a Beckman Coulter Allegra 25R Centrifuge using a TA-10.250 rotor. The cell pellet was washed twice in ice cold glycerol (10% in dH_2O), incubated on ice for 5 min and centrifuged at 8,000 rpm for 5 min at 4˚C. The cell pellet was resuspended in 500 µl ice cold glycerol (10% in dH_2O), and 50 µl aliquots were stored at -80˚C until use.

3.2.2.3 Construction of *E. coli* deletion strains expressing *C. jejuni 1291*

The *Cj 1291* gene was codon optimized (*1291CO)* for expression in *E. coli* using the Integrated Gene Technologies (IDT) codon optimization tool, as *Cj* contains codons not expressed in *E. coli* (129). A full outline of codon differences between the *1291* and *1291CO* genes is provided in Appendix A.1 (Table A.1.1). *1291CO* was synthesized by IDT and amplified by PCR using iProof (Bio-Rad) with 1291CO-L2 and 1291CO-R2 primers to yield a 1545 bp product. The PCR product was digested with *XbaI* and *MfeI* (NEB) and ligated to the pRRC plasmid (129) digested using *XbaI* and *MfeI* to create the *1291CO*_pRRC construct. The construct was transformed into *E. coli* DH5α and selected on chloramphenicol. The *1291CO*_pRRC plasmid was purified using the EZ-10 Spin Column Plasmid DNA Minipreps Kit for Low Copy (BioBasic) to verify construction via PCR analysis using iProof and sequencing with the primers cat4, which binds 395 bp upstream of the *1291CO* gene on the pRRC plasmid, and pRRC-REV1, which binds 232 bp downstream of the *1291CO* gene on the pRRC plasmid.

To create the cross-complemented *E. coli* cell lines expressing *1291CO*, 368 ng *1291CO*_pRRC purified from *E. coli* DH5α via miniprep (BioBasic), was transformed into 50 µl aliquots of electrocompetent amidase activator deficient *E. coli* strains (Δ*envC*, Δ*nlpD*, and Δ*envC*Δ*nlpD*) via electroporation using an ECM630 Electro Cell Manipulator (BTX) with the voltage set at 1750V, the resistor set at 200 Ω, and the capacitor set at 25 µF. Successfully transformed colonies were selected on kanamycin and chloramphenicol plates. The presence of the plasmid in transformed strains was confirmed via PCR analysis using iProof of plasmid minipreps with the cat4/pRRC-REV1 and 1291CO-L2/1291CO-R2 primer pairs.

3.2.2.4 Construction of *C. jejuni* Δ*1291* expressing *E. coli envC*

The *envC* gene was PCR amplified using iProof from WT *E. coli* strain TB28 gDNA extracted as described previously (Chapter 2, Section 2.2.2), with EnvC-F and EnvC-R primers to yield a 1325 bp product. The PCR product was digested with *XbaI* and *EcoRI* (NEB) and ligated to the pRRC plasmid digested using *XbaI* and *MfeI* (NEB) to create the *envC*_pRRC construct. The construct was transformed into *E. coli* DH5α and selected on chloramphenicol plates. The *envC*_pRRC plasmid was purified by plasmid miniprep to verify construction via PCR analysis using iProof and sequencing with the primers cat4, which binds 170 bp upstream of the *envC* gene on the pRRC plasmid, and pRRC-REV1, which binds 178 bp downstream of the *envC* gene on the pRRC plasmid.

To create the cross-complemented *Cj* Δ*1291* strain expressing *E. coli envC*, 1.8 µg of the *envC*_pRRC construct purified by plasmid miniprep was naturally transformed into *Cj* Δ*1291* and selected on kanamycin and chloramphenicol plates. Genomic DNA was extracted to confirm the genotype via PCR analysis using iProof and sequencing with the primer pairs cat4/pRRC-REV1

to verify the presence of the *envC*_pRRC construct in the genome, and the forward primers ak233, ak234, and ak235, each with the reverse primer ak237 to determine into which rRNA spacer region the construct was inserted. The construct was found to have been integrated into the ak235 site (data not shown).

3.2.3 Microscopy

3.2.3.1 Slide preparation

Slides were prepared as described in Chapter 2, Section 2.2.4.

3.2.3.2 Direct interference contrast microscopy

E. coli strains grown overnight in selective LB broth were diluted to an OD_{600} of 0.05 in LB broth and grown until the OD_{600} was between 0.4 and 0.7. *Cj* strains were prepared as described in Chapter 2, Section 2.2.4. Cultures were live mounted on agarose pads and the cells were imaged on a Nikon Eclipse TE2000-U microscope equipped with a 100X oil immersion objective lens and a Hamamatsu Orca camera system.

3.2.3.3 *E. coli* membrane staining

The *E. coli* membrane staining protocol was adapted from Uehara *et al*. (105). *E. coli* cultures were grown as described for DIC microscopy above. FM1-43FX membrane stain (Invitrogen) in DMSO (10 µg/ml) was added to the broth cultures and incubated on ice in the dark for 10 min. Cultures were live mounted on agarose pads and the cells were imaged using the blue filter for fluorescence microscopy equipped on the Nikon Eclipse TE2000-U microscope.

3.3 Results

3.3.1 Bioinformatic analyses

Unlike *E. coli*, the *Cj* genome encodes for only one amidase (*cjj81176_1285*; *amiA*) and one protein containing an M23 peptidase family (pfam) domain (*cjj81176_1291*; *1291*). Predicted gene domain analysis of *1291* revealed domain similarity to the amidase activators *envC* and *nlpD* from both *E. coli* and *V. cholerae* (Appendix A.1, Figure A.1.2). However, *1291* shows more gene domain homology to *envC* than *nlpD* as *1291* is predicted to have coiled coil regions which are present in *envC* but not in *nlpD* and lacks the PG binding LysM domain present in *nlpD* but not in *envC* (Appendix A.1, Figure A.1.2, 113). The amino acid residues in 1291 show greater similarity to EnvC than NlpD in *E. coli* with 22% identity/52% similarity to *E. coli* EnvC (Appendix A.1, Figure A.1.3), compared to 19% identity/48% similarity to *E. coli* NlpD (data not shown). 1291 also shows greater homology to *E. coli* EnvC with an E value of 2×10^{-9} as determined by protein BLAST (National Center for Biotechnology information), than *E. coli* NlpD with an E value of 3×10^{-7}. The predicted three-dimensional protein structure of 1291 determined by the online program Swiss-Model was based on the crystal structure of *E. coli* EnvC solved by Cook *et al*. (147), which showed that EnvC contained three coiled coil regions separated by disordered regions, followed by the LytM domain (Appendix A.1 Figure A.1.4A). Protein domain analysis using the EMBL-EBI program HMMER revealed that in addition to a signal peptide (amino acid residues 1-22), which was also shown in the gene domain analysis described above (Appendix A.1, Figure A.1.2), the 1291 protein possessed three coiled coil regions (amino acids 19-50, 58-106, and 163-235) separated by regions of disorder, followed by an N-terminal LytM domain (amino acids 312-377) (Appendix A.1, Figure A.1.4B). Therefore, the HMMER protein domain analysis suggests that the 1291 protein may indeed resemble the Swiss-Model predicted structure

(Appendix A.1, Figure A.1.4) and thus look similar to *E. coli* EnvC. Like *E. coli* EnvC, *Cj* 1291 also lacks endopeptidase proteolytic residues in its LytM domain (117). However, the 1291 LytM domain contains conserved amidase-binding residues identified in *E. coli* EnvC, notably *Cj* 1291 phenylalanine 300, asparagine 301, and valines 305 and 355, corresponding to *E. coli* EnvC tryptophan 320, lysine 321, and valines 324 and 353, respectively (Appendix A.1, Figure A.1.3, 117). In addition, the LytM domains of 1291 and EnvC show 23% identity/65% similarity (Appendix A.1, Figure A.1.3). The sequence similarity, conserved binding residues, and overall domain structure led me to hypothesize that 1291 may be a homologue of *E. coli* EnvC.

3.3.2 *E. coli* strain morphologies match those previously reported

To confirm overall cell morphology of *E. coli* TB28, Δ*envC*, Δ*nlpD*, and Δ*envC*Δ*nlpD*, both DIC images and images of FM1-43FX stained cells were taken. The DIC images showed that all *E. coli* strains matched morphologies previously published by the Bernhardt lab (105, 111) where Δ*envC* and Δ*nlpD* showed some short cell chains (3-4 cells) while most cells resembled the WT TB28 strain, and the Δ*envC*Δ*nlpD* strain showed extremely long chains with fairly regularly spaced septa extending off the field of view (Figure 3.1). Imaging with the FM1-43FX membrane stain confirmed the presence of dividing cells in the WT TB28 strain, as well as the formation of fully formed septa in the short chains formed by Δ*envC* and Δ*nlpD* and in the long chains of Δ*envC*Δ*nlpD,* also as observed previously (105, 111) (Figure 3.2).

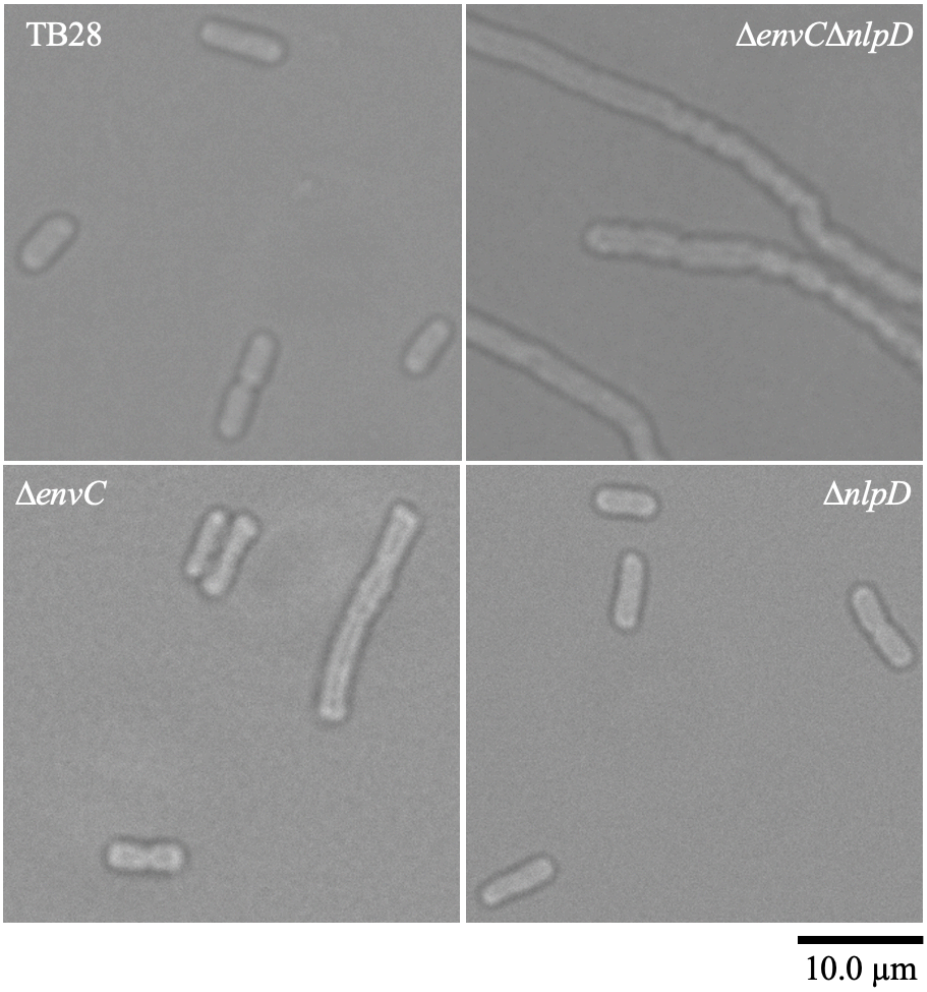

Figure 3.1 Cellular morphology of the *E. coli* strains Δ*envC*, Δ*nlpD*, Δ*envC*Δ*nlpD*, and the wild type strain TB28. Strains were imaged by DIC microscopy at 100X magnification.

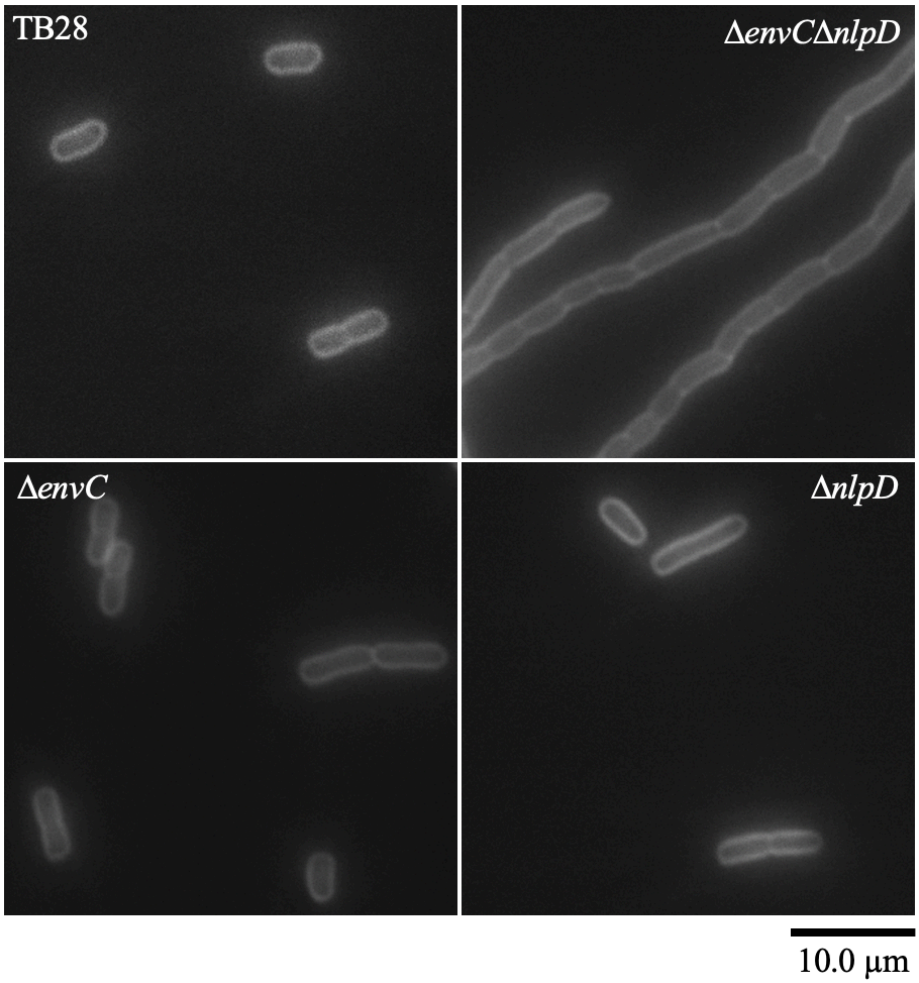

Figure 3.2 Cellular morphology of *E. coli* TB28, Δ*envC*, Δ*nlpD*, and Δ*envC*Δ*nlpD* strains as visualized by FM1-43FX membrane stain. Cells were stained with 10 µg/ml FM1-43FX in DMSO, and images were captured at 100X magnification using a blue fluorescence filter.

3.3.3 Addition of *E. coli envC* to *C. jejuni* Δ*1291* shows some phenotypic complementation

The introduction of *envC* to Δ*1291* showed a clear reduction in the amount of long chain-like cells characteristic of *Cj* Δ*1291* (Figure 3.3A). On average, the cells still appeared to be longer than WT *Cj*, but some complementation was clearly observed. When cells from the frozen stock Δ*1291* + *envC* strain were pulled for a second time, there appeared to be an increase in the number of longer cells than was observed when the strain was initially imaged (Figure 3.3B).

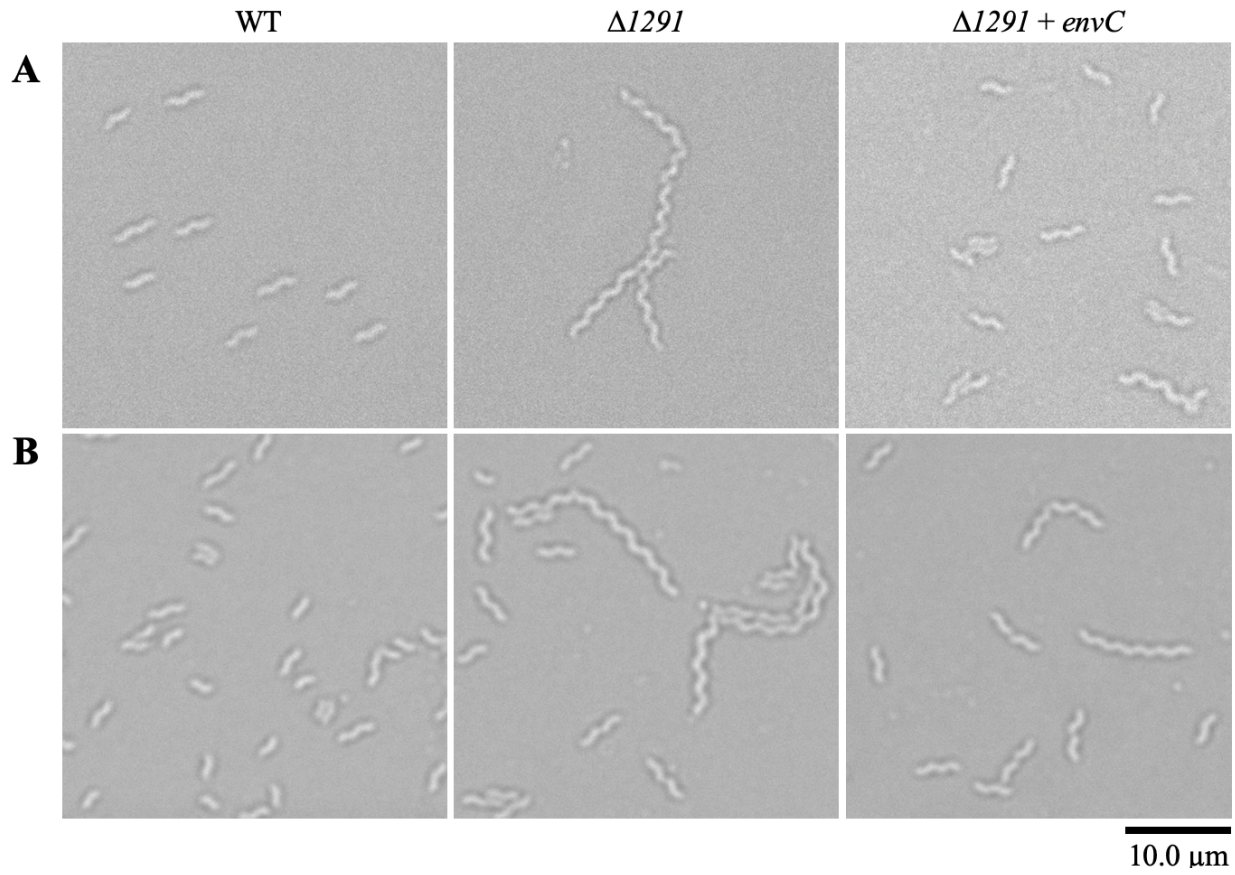

Figure 3.3 Cellular morphology of *Cj* Δ*1291* expressing *E. coli envC.* WT, Δ*1291* and Δ*1291* expressing *envC* (Δ*1291* + *envC*) strains were imaged by DIC microscopy at 100X magnification. A) The freshly transformed Δ*1291* + *envC* strain showed more phenotype complementation than B) when the strain had been removed from the freezer a second time.

3.3.4 Addition of *1291CO* to the *E. coli* double amidase activator deletion strain shows phenotypic complementation

The introduction of *1291CO* to the *E. coli* single amidase activator deletion strains, Δ*envC* and Δ*nlpD*, did not appear to alter the overall cell morphology in any significant way (Figure 3.4). This result was expected as Δ*envC* and Δ*nlpD* each have one functional *E. coli* amidase activator present in the cells and both strains already have overall cell morphologies similar to the WT strain TB28.

When *1291CO* was added to the *E. coli* double amidase activator deletion strain Δ*envC*Δ*nlpD*, a clear reduction in the amount of cell chains was observed when cultures were grown consistently in media containing chloramphenicol (Figure 3.4).

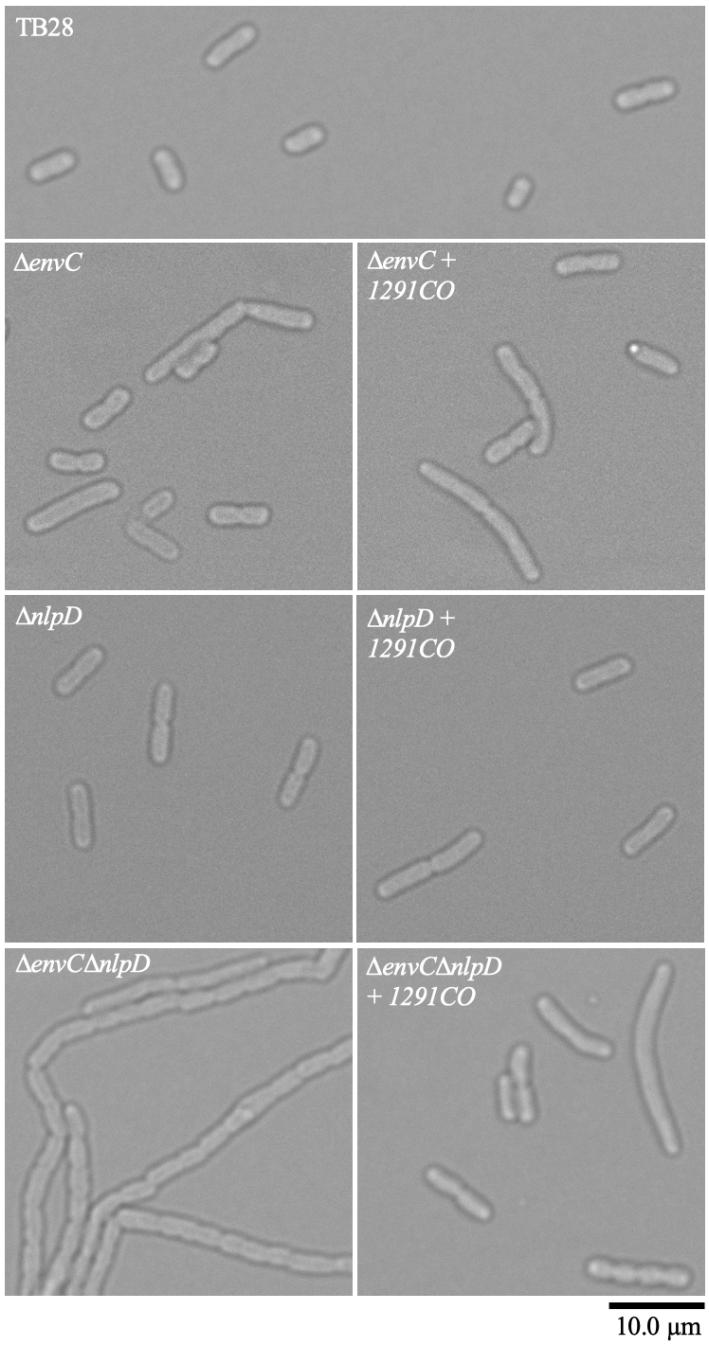

Figure 3.4 Cellular morphology of *E. coli* amidase activator deletion strains expressing the codon optimized *1291* gene in the pRRC plasmid. Cells were imaged by DIC microscopy at 100X magnification. The Δ*envC*Δ*nlpD* + *1291CO* strain was grown only in media containing chloramphenicol.

3.4 Discussion

In this study, *Cj 1291* was cross-complemented into *E. coli* amidase activator deficient strains, and the *E. coli* amidase activator *envC* was cross-complemented into Δ*1291* to determine if 1291 could perform a homologous function to the *E. coli* amidase activator EnvC. Cross-complementation studies of PG hydrolases or proteins associated with PG hydrolases (e.g., amidase activators) are rare, with the only other study, to my knowledge, finding that *Chlamydia pneumoniae* AmiA was able to restore daughter cell separation in an *E. coli* mutant lacking all three *E. coli* amidases (148).

The introduction of *envC* to Δ*1291* showed morphological complementation, however repeated removal of the stock strain from the freezer resulted in an increase of long chain-like cells although there was still some complementation visually observed compared to Δ*1291* (Figure 3.3). As this was a qualitative, not quantitative, study, the exact difference between the complementation in Figure 3.3A and Figure 3.3B could not be determined. CellTool analysis could be used in future studies to quantify the degree of complementation by *envC* in Δ*1291* and could reveal the degree to which complementation is lost over repeated removal from the freezer.

When *1291CO* was complemented into *E. coli* Δ*envC*Δ*nlpD*, the reversion to WT *E. coli* cell morphology was only observed for cultures grown consistently in media containing chloramphenicol (Figure 3.4). Cultures of Δ*envC*Δ*nlpD* + *1291CO* that were confirmed to be expressing the *1291CO*_pRRC plasmid and imaged using the method described in Section 3.2.3, where cultures are grown over-day in broth lacking antibiotics, showed the long-chained phenotype indicative of Δ*envC*Δ*nlpD* (Appendix A.1, Figure A.1.5). In addition, the Δ*envC*Δ*nlpD* + *1291CO* stock culture only grew once after freezing in LB with glycerol at -80˚C, meaning the strain needed to be retransformed for each assay. Therefore, it appears that the *1291CO*_pRRC

plasmid is somehow toxic to the *E. coli* Δ*envC*Δ*nlpD* strain, as the strain seemed to reject the plasmid and revert to its chained phenotype when it was no longer in need of chloramphenicol resistance, whether that be during growth in an over-day culture, or after repeated removal from the freezer. *1291CO* did not appear to be toxic to *E. coli* as the Δ*envC* and Δ*nlpD* strains kept the plasmid and chloramphenicol resistance after repeated removal from the freezer. Δ*envC*Δ*nlpD* was a fairly unhealthy mutant strain as it grew much more slowly than Δ*envC* and Δ*nlpD* (data not shown), which may be a factor in its intolerance of *1291CO*_pRRC in the absence of chloramphenicol, despite the complementation of cell division conferred by 1291CO.

This study revealed that the *Cj* LytM protein 1291 was able to complement the severe chaining phenotype of an *E. coli* strain lacking the critical cell division LytM proteins EnvC and NlpD (Figure 3.4). As these LytM proteins appeared to sufficiently activate cross-species amidases and show domain and sequence homology, it can be hypothesized that their binding and activating mechanisms function similarly.

In *E. coli*, it has been shown that the C-terminal coiled coil region of EnvC is involved in recruitment to the division site (111), while the N-terminal coiled coil domain, termed the "restraining arm", appears to act as an autoinhibitory mechanism as it blocks the residues in the LytM domain involved in amidase activation (147). At the division site, EnvC binds to the periplasmic domain of the transmembrane protein FtsX in complex with FtsE (147). EnvC's interaction with FtsEX, as well as the ATPase activity of FtsEX, are required for amidase activation and daughter cell separation as the FtsEX complex is involved in the coordination of PG remodelling and cytoplasmic cell division events (149-151). It has been suggested that EnvC is able to activate downstream amidases through a mechanical conformational change brought about through the EnvC C-terminal coiled coil domain binding with FtsX which releases the

restraining arm from the LytM domain, thus exposing the residues involved in amidase activation to amidases at the division site (147). EnvC and FtsEX have also been shown to interact in other Gram-negative bacteria (151). A binding interaction between 1291 and FtsX has not yet been demonstrated, however in the *Cj* genome, *ftsX* (*1292*) is located immediately upstream of *1291*. Together, the bioinformatic analyses and *E. coli* cross-complementation study data lead to a strong hypothesis that like *E. coli* EnvC, 1291 binds the periplasmic FtsX domain, which induces a conformational change in 1291 that liberates the LytM domain amidase binding site from the autoinhibitory N-terminal coiled coil domain.

The partial complementation observed when the LytM proteins 1291 and EnvC were complemented into heterologous Gram-negative organisms showed that 1291 was able to perform a homologous function to EnvC/NlpD by activating the *E. coli* amidases thus restoring cell separation. However, further studies will be needed to confirm the mechanism for 1291 activation of AmiA in *Cj*.

Chapter 4: Conclusion

C. jejuni is often the leading cause of food-borne bacterial gastroenteritis in humans in the developed world, and it is becoming increasingly resistant to commonly used antibiotics (1). There are currently only a few established disease-susceptible animal models that mimic human campylobacteriosis pathology, though many have been developed that require enhanced susceptibility via genetic or environmental modifications (83, 123-128). Therefore, *in vitro* characterization of putative *Cj* pathogenesis factors is critical to further our current understanding of this prevalent human pathogen.

This study focused on the analysis of the *C. jejuni* shape determinant *1291* in cell morphology, biology, and pathogenesis, and I hypothesized that 1291 was involved in *C. jejuni* morphological changes, and therefore pathogenesis, by activating the PG amidase AmiA.

My first aim, the *in vitro* characterization of *1291*, was reported in Chapter 2. The deletion of *1291* resulted in a long chained or filamented cellular phenotype similar to the *amiA* deletion strain morphology observed previously in our lab (99). This indicates that 1291 is indeed involved in *Cj* morphological changes, and that 1291 and AmiA may be involved in the same, or similar, pathway. Deletion of *1291* also resulted in severe motility and autoagglutination defects, an increase in biofilm formation, and a change in cell surface carbohydrates. Therefore, there is evidence to support the involvement of *1291* in pathogenesis as its absence affects key pathogenesis-associated attributes in *Cj*. Future research could look at the mechanisms underlying the phenotypic changes observed for Δ*1291*. The degree of envelope stress in the Δ*1291* strain could be assessed by examining the level of cell lysis via SDS-PAGE and Western Blot analysis of culture supernatants compared to WT. To determine if excess eDNA is released due to an increase in envelope stress in Δ*1291*, eDNA from the cell-free supernatant of biofilm cultures

could be quantified via qPCR. The transition to coccoid formation in Δ*1291* was not assessed in this study, however since Δ*amiA* exhibited a defect in this transition (99), demonstrating a coccoid formation defect in Δ*1291* would provide another link between the function of 1291 and AmiA.

In other pathogenic bacteria, LytM domain-containing proteins have proven important both in cell separation and pathogenesis (107, 120, 152), as this study demonstrated in Chapter 2 was likely true for 1291. Though the chained phenotype of Δ*1291* has not yet been confirmed, the morphological similarities between the Δ*1291* and the previously described chained Δ*amiA* mutant strain (Chapter 2, 99), and the ability of 1291 to reverse the cell division defect in *E. coli* lacking both amidase activators (Chapter 3), point to a chained phenotype indicative of a defect in cell separation for Δ*1291*. However, to definitively determine the cell morphology of Δ*1291*, transmission electron microscopy at the same magnification used to visualize septa in Δ*amiA* could be used to visualize septa in Δ*1291* (99). Staining with the fluorescent D-alanine analogue HADA, which specifically labels PG (153), could also be used to visualize septa in Δ*1291* as it has previously highlighted the presence of septal PG in the chained *H. pylori* mutant, Δ*amiB* (107).

My second aim, cross-complementation of *C. jejuni 1291* and *E. coli envC*, was reported in Chapter 3. The addition of a codon optimized version of *1291* into the *E. coli* double amidase activator deletion strain, Δ*envC*Δ*nlpD*, showed complementation by reducing the occurrence of long cell chains, which was also seen upon addition of *envC* into the *1291* deletion strain. While in each case the cell morphology did not completely revert to wild type, the complementation shown by each LytM protein in a heterologous Gram-negative bacterium showed that 1291 can perform a homologous function to EnvC/NlpD in *E. coli* cells by activating the *E. coli* amidases. Therefore, the cross-complementation study provides evidence to support the activation of amidases by 1291 and its involvement in cell division.

The lack of quantifiable data from the cross-complementation assay in Chapter 3 is a limiting factor of this study. It would not be feasible to perform CellTool analysis on *E. coli* Δ*envC*Δ*nlpD* due to the length of the cell chains which were typically touching or overlapping and extended off the microscope frame. However, quantification could be performed for *1291CO* in Δ*envC* or Δ*nlpD* to determine if there were slight phenotypic changes upon addition of *1291CO*, as well as for *envC* in Δ*1291* to quantify the degree of complementation and to reveal the degree to which complementation is lost over repeated removal from the freezer.

Running concurrently with my project, the Gaynor lab designed and purified protein constructs of the 1291 LytM domain and the C-terminal active domain of AmiA. These proteins were sent to Newcastle University, and there, with the help of Dr. Waldemar Vollmer and his lab, they will be used to assess the activity of the AmiA protein on PG in the presence and absence of 1291 via an HPLC-based assay. This will enable us to determine biochemically if the PG hydrolysis by AmiA is enhanced in the presence of 1291, which would indicate 1291 functions as an AmiA activator. Protein pull-down assays or bacterial two-hybrid assays would also be useful for confirming a protein binding interaction between 1291 and AmiA, as well as between 1291 and FtsX. If our data suggest 1291 and AmiA undergo a binding interaction, point mutations could be constructed in the 1291 LytM domain in the four residues predicted to be critical for amidase binding (Appendix A.1, Figure A.1.3). This would allow us to determine if these residues are critical for binding to AmiA, and if there are additional unknown key binding residues present in the 1291 LytM domain. Expressing a truncated protein containing only the 1291 LytM domain in Δ*1291* could reveal the presence of a self-inhibitory mechanism if the LytM domain alone caused extreme toxicity, as was shown previously with a truncated *E. coli* EnvC protein lacking all coiled coil domains (111).

A strength of this project was that the *in vitro* phenotypic data in Chapter 2 was collected through the use of assays standard to the Gaynor lab. These assays have been used to characterize many past mutant strains and as such, we can easily compare the data collected from this project to any previously described mutant strain(s) to aid in the identification of trends or correlations between deleted genes. The cross-complementation assay in Chapter 3 was designed to be a straightforward study to either support or refute the hypothesis that 1291 is involved in the activation of AmiA. Overall, the assays used in this project, with the exception of the hydrophobicity assay, all yielded clear results for data analysis.

The most evident limitation in this study overall, is the lack of *in vivo* data. The Gaynor lab does not currently have the resources required to work with either the chick colonization model (82) or one of the novel campylobacteriosis mouse models (83, 123-128), so a collaboration with a group possessing the necessary resources would be required to obtain *in vivo* data. Observing the pathogenicity of Δ*1291 in vivo* will be crucial for determining its candidacy as a target for antimicrobials.

Overall, this research has helped to better understand the role of cell division and morphology factors in *Cj* biology and has provided evidence that the LytM-domain containing protein 1291 acts as a *Cj* pathogenesis factor and performs a homologous function to *E. coli* EnvC/NlpD.

References

1. Kaakoush, N. O., Castaño-Rodriguez, N., Mitchell, H. M., and Man, S. M. 2015. Global epidemiology of *Campylobacter* infection. *Clin Microbiol Rev* 28: 687-720.

2. Black, R. E., Levine, M. M., Clements, M. L., Hughes, T. P., and Blaser, M. J. 1988. Experimental *Campylobacter jejuni* infection in humans. *J Infect Dis* 157(3): 472-479.

3. Tribble, D. R., Baqar, S., Scott, D. A., Oplinger, M. L., Trespalacio, F., Rollins, D., Walker, R. I., Clements, J. D., Walz, S., Gibbs, P., Burg III, E. F., Moran, A. P., Applebee, L., and Bourgeois, A. L. 2010. Assessment of the duration of protection in *Campylobacter jejuni* experimental infection in humans. *Infect Immun* 78(4): 1750-1759.

4. Kirkpatrick, B. D., Lyon, C. E., Porter, C. K., Maue, A. C., Guerry, P., Pierce, K. K., Carmolli, M. P., Riddle, M. S., Larsson, C. J., Hawk, D., Dill, E. A., Fingar, A., Poly, F., Fimlaid, K. A., Hoq, F., and Tribble, D. R. 2013. Lack of homologous protection against *Campylobacter jejuni* CG8421 in a human challenge model. *Clin Infect Dis* 57(8): 1106-1113.

5. Bacon, D. J., Alm, R. A., Burr, D. H., Hu, L., Kopecko, D. J., Ewing, C. P., Trust, T. J., and Guerry, P. 2000. Involvement of a plasmid in virulence of *Campylobacter jejuni* 81-176. *Infect Immun* 68(8): 4384-4390.

6. Bacon, D. J., Szymanski, C. M., Burr, D. H., Silver, R. P., Alm, R. A., and Guerry, P. 2001. A phase-variable capsule is involved in virulence of *Campylobacter jejuni* 81-176. *Mol Microbiol* 40(3): 769-777.

7. Everest, P. H., Goossens, H., Butzler, J.-P., Lloyd, D., Knutton, S., Ketley, J. M., and Williams, P. H. 1992. Differentiated Caco-2 cells as a model for enteric invasion by *Campylobacter jejuni* and *C. coli*. *J Med Microbiol* 37: 319-325.

8. Mellits, K. H., Mullen, J., Wand, M., Armbruster, G., Patel, A., Connerton, P. L., Skelly, M., and Connerton, I. F. 2002. Activation of the transcription factor NF-*κ*B by *Campylobacter jejuni*. *Microbiology* 148: 2753-2763.

9. Al-Sayeqh, A. F., Loughlin, M. F., Dillon, E., Mellits, K. H., and Connerton, I. F. 2010. *Campylobacter jejuni* activates NF-*κ*B independently of TLR2, TLR4, Nod1 and Nod2 receptors.

10. van Putten, J. P., van Alphen, L. B., Wosten, M. M., and de Zoete, M. R. 2009. Molecular mechanisms of *Campylobacter* infection. *Curr Top Microbiol Immunol* 337: 197-229.

11. Hickey, T. E., McVeigh, A. L., Scott, D. A., Michielutti, R. E., Bixby, A., Carroll, S. A., Bourgeois, A. L., and Guerry, P. 2000. *Campylobacter jejuni* cytolethal distending toxin mediates interleukin-8 from intestinal epithelial cells. *Infect Immun* 68(12): 6535-6541.

12. Hu, L., Bray, M. D., Osorio, M., Kopecko, D. J. 2006. *Campylobacter jejuni* induces maturation and cytokine production in human dendritic cells. *Infect Immun* 74(5): 2697-2705.

13. Rathinam, V. A. K., Hoag, K. A., and Mansfield, L. S. 2008. Dendritic cells from C57BL/6 mice undergo activation and induce Th1-effector cell responses against *Campylobacter jejuni*. *Microbes Infect* 10: 1316-1324.

14. Karlinger, K., Gyorke, T., Mako, E., Mester, A., and Tarjan, Z. 2000. The epidemiology and the pathogenesis of inflammatory bowel disease. *Eur J Radiol* 35: 154-167.

15. Nachamkin, I., Allos, B. M., and Ho, T. 1998. *Campylobacter* species and Guillain-Barré syndrome. *Clin Microbiol Rev* 11: 555-567.

16. Keithlin, J., Sergeant, J., Thomas, M. K., and Fazil, A. 2014. Systematic review and meta-analysis of the proportion of *Campylobacter* cases that develop chronic sequelae. *BMC Public Health* 14: 1203.

17. Heikema, A. P., Islam, Z., Horst-Kreft, D., Huizinga, R., Jacobs, B. C., Wagenaar, J. A., Poly, F., Guerry, P., van Belkum, A., Parker, C. T., and Endtz, H. P. 2015. *Clin Microbiol Infect* 21: 852.e1-852.e9.

18. Lecuit, M., Abachin, E., Martin, A., Poyart, C., Pochart, P., Suarez, F., Bengoufa, D., Feuillard, J., Lavergne, A., Gordon, J. I., Berche, P., Guillevin, L., and Lortholary, O. 2004. Immunoproliferative small intestinal disease associated with *Campylobacter jejuni*. *N Engl J Med* 350: 239-248.

19. Lee, M. D., and Newell, D. G. 2006. *Campylobacter* in poultry: Filling an ecological niche. *Avian Dis* 50: 1-9.

20. Mylius, S. D., Nauta, M. J., and Havelaar, A. H. 2007. Cross-contamination during food preparation: A mechanistic model applied to chicken-borne *Campylobacter*. *Risk Anal* 27: 803-813.

21. Mohan, V. 2015. Faeco-prevalence of *Campylobacter jejuni* in urban wild birds and pets in New Zealand. *BMC Res Notes* 8: 1.

22. Ramonaite, S., Novoslavskij, A., Zakariene, G., Aksomaitiene, J., Malakauskas, M. 2015. High prevalence and genetic diversity of *Campylobacter jejuni* in wild crows and pigeons. *Curr Microbiol* 71: 559-565.

23. Bahrndorff, S., Garcia, A. B., Vigre, H., Nauta, M., Heegaard, P. M. H., Madsen, M., Hoorfar, J., and Hald, B. 2015. Intestinal colonization of broiler chickens by *Campylobacter* spp. in an experimental infection study. *Epidemiol Infect* 143: 2381-2389.

24. Pielsticker, C., Glünder, G., Aung, Y., and Rautenschlein, S. 2016. Colonization pattern of *C. jejuni* isolates of human and avian origin and differences in the induction of immune responses in chicken. *Vet Immunol Immunopathol* 169: 1-9.

25. Clark, C. G., Price, L., Ahmed, R., Woodward, D. L., Melito, P. L., Rodgers, F. G., Jamieson, F., Cieben, B., Li, A., and Ellis, A. 2003. Characterization of waterborne outbreak-associated *Campylobacter jejuni*, Walkerton, Ontario. *Emerg Infect Dis* 9(10): 1232-1241.

26. Korlath, J. A., Osterholm, M. T., Judy, L. A., Forfang, J. C., and Robinson, R. A. 1985. A point-source outbreak of campylobacteriosis associated with consumption of raw milk. *J Infect Dis* 152(3): 592-596.

27. Moffatt, C. R. M., Greig, A., Valcanis, M., Gao, W., Seemann, T., Howden, B.P., and Kirk, M. D. 2016. A large outbreak of *Campylobacter jejuni* infection in a university college caused by chicken liver pâté, Australia, 2013. *Epidemiol Infect* 144: 2971-2978.

28. Hofreuter, D., Tsai, J., Watson, R. O., Novik, V., Altman, B., Benitez, M., Clark, C., Perbost, C., Jarvie, T., Du, L., and Galán, J. E. 2006. Unique features of a highly pathogenic *Campylobacter jejuni* strain. *Infect Immun* 74(8): 4694-4707.

29. Parkhill, J., Wren, B. W., Mungall, K., Ketley, J. M., Churcher, C., Basham, D., Chillingworth, T., Davies, R. M., Feltwell, T., Holroyd, S., Jagels, K., Karlyshev, A. V., Moule, S., Pallen, M. J., Penn, C. W., Quail, M. A., Rajandream, M.-A., Rutherford, K. M., van Vliet, A. H. M., Whitehead, S., and Barrell, B. G. 2000. The genome sequence of the food-borne pathogen *Campylobacter jejuni* reveals hypervariable sequences. *Nature* 403: 665-668.

30. Konkel, M. E., Klena, J. D., Rivera-Amill, V., Monteville, M. R., Biswas, D., Raphael, B., and Mickelson, J. 2004. Secretion of virulence proteins from *Campylobacter jejuni* is dependent on a functional flagellar export apparatus. *J Bacteriol* 186(11): 3296-3303.

31. Barrero-Tobon, A. M., and Hendrixson, D. R. 2012. Identification and analysis of flagellar coexpressed determinants (Feds) of *Campylobacter jejuni* involved in colonization. *Mol Microbiol* 84(2): 352-369.

32. Watson, R. O., and Galán, J. E. 2005. Signal transduction in *Campylobacter jejuni*-induced cytokine production. *Cell Microbiol* 7(5): 655-665.

33. Gaynor, E. C., Wells, D. H., MacKichan, J. K., and Falkow, S. 2005. The *Campylobacter jejuni* stringent response controls specific stress survival and virulence-associated phenotypes. *Mol Microbiol* 56(1): 8-27.

34. Szymanski, C. M., and Gaynor, E. C. 2012. How a sugary bug gets through the day: Recent developments in understanding fundamental processes impacting *Campylobacter jejuni* pathogenesis. *Gut Microbes* 3(2): 135-144.

35. Palyada, K., Sun, Y.-Q., Flint, A., Butcher, J., Naikare, H., and Stintzi, A. 2009. Characterization of the oxidative stress stimulon and PerR regulon of *Campylobacter jejuni*. *BMC Genomics* 10: 481.

36. Gaasbeek, E. J., van der Wal, F. J., van Putten, J. P. M., de Boer, P., van der Graaf-van Bloois, L., de Boer, A. G., Vermaning, B. J., and Wagenaar, J. A. 2009. Functional characterization of excision repair and RecA-dependent recombination DNA repair in *Campylobacter jejuni*. *J Bacteriol* 191(12): 3785-3793.

37. Gilbreath, J. J., Cody, W. L., Merrell, D. S., Hendrixson, D. R. 2011. Change is good: Variations in common biological mechanisms in the epsilonproteobacterial genera *Campylobacter* and *Helicobacter. Microbiol Mol Biol Rev* 75(1): 84-132.

38. Silva, J., Leite, D., Fernandes, M., Mena, C., Gibba, P. A., and Teixeira, P. 2011. *Campylobacter* spp. as a foodborne pathogen: A review. *Front Microbiol* 2. Article 200.

39. Frirdich, E., Biboy, J., Adams, C., Lee, J., Ellermeier, J., Gielda, L. D., DiRita, V. J., Girardin, S. E., Vollmer, W., and Gaynor, E. C. 2012. Peptidoglycan-modifying enzyme Pgp1 is required for helical cell shape and pathogenicity traits in *Campylobacter jejuni*. *PLoS Pathog* 8(3): e1002602.

40. Hendrixson, D. R. 2006. A phase-variable mechanism controlling the *Campylobacter jejuni* FlgR response regulator influences commensalism. *Mol Microbiol* 61(6): 1646-1659.

41. Hendrixson, D. R. 2008. Restoration of flagellar biosynthesis by varied mutational events in *Campylobacter jejuni*. *Mol Microbiol* 70(2): 519-536.

42. Bayliss, C. D., Bidmos, F. A., Anjum, A., Manchev, V. T., Richards, R. L., Grossier, J.-P., Wooldridge, K. G., Ketley, J. M., Barrow, P. A., Jones, M. A., and Tretyakov, M. V. 2012. Phase variable genes of *Campylobacter jejuni* exhibit high mutation rates and specific mutational patterns but mutability is not the major determinant of population structure during host colonization. *Nucleic Acids Res* 40(13): 5876-5889.

43. Wassenaar, T. M. 2002. Genetic differentiation of *Campylobacter jejuni*. *Int J Infect Dis* 6: 3S22-3S25.

44. Cameron, A., Huynh, S., Scott, N. E., Frirdich, E., Apel, D., Foster, L. J., Parker, C. T., and Gaynor, E. C. 2015. High-frequency variation of purine biosynthesis genes is a mechanism of success in *Campylobacter jejuni*. *mBio* 6(5): e00612-15.

45. Frirdich, E., Biboy, J., Huynh, S., Parker, C. T., Vollmer, W., and Gaynor, E. C. 2017. Morphology heterogeneity within a *Campylobacter jejuni* helical population: The use of calcofluor white to generate rod-shaped *C. jejuni* 81-176 clones and the genetic determinants responsible for differences in morphology within 11168 strains. *Mol Microbiol* 104(6): 948-971.

46. Guerry, P., Szymanski, C. M., Prendergast, M. M., Hickey, T. E., Ewing, C. P., Pattarini, D. L., and Moran, A. P. 2002. Phase variation of *Campylobacter jejuni* 81-176 lipooligosaccharide affects ganglioside mimicry and invasiveness in vitro. *Infect Immun* 70(2): 787-793.

47. Szymanski, C. M., Logan, S. M., Linton, D., and Wren, B. W. 2003. *Campylobacter* – a tale of two protein glycosylation systems. *Trends Microbiol* 11(5): 233-238.

48. Thibault, P., Logan, S. M., Kelly, J. F., Brisson, J.-R., Ewing, C. P., Trust, T. J., and Guerry, P. 2001. Identification of the carbohydrate moieties and glycosylation motifs in *Campylobacter jejuni* flagellin. *J Biol Chem* 276(37): 34862-34870.

49. Karlyshev, A. V., Champion, O. L., Churcher, C., Brisson, J.-R., Jarrell, H. C., Gilbert, M., Brochu, D., St Michael, F., Li, J., Wakarchuk, W. W., Goodhead, I., Sanders, M., Stevens, K., White, B., Parkhill, J., Wren, B. W., and Szymanski, C. M. 2005. Analysis of *Campylobacter jejuni* capsular loci reveals multiple mechanisms for the generation of structural diversity and the ability to form complex heptoses. *Mol Microbiol* 55(1): 90-103.

50. van Mourik, A., Steeghs, L., van Laar, J., Meiring, H. D., Hamstra, H.-J., van Putten, J. P. M., and Wösten, M. M. S. M. 2010. Altered linkage of hydroxyacyl chains in lipid A of *Campylobacter jejuni* reduces TLR4 activation and antimicrobial resistance. *J Biol Chem* 285(21): 15828-15836.

51. O'Toole, G., Kaplan, H. B., and Kolter, R. 2000. Biofilm formation as microbial development. *Annu Rev Microbiol* 54: 49-79.

52. Donlan, R. M. 2002. Biofilms: Microbial life on surfaces. *Emerg Infect Dis* 8(9): 881-890.

53. Branda, S. S., Vik, A., Friedman, L., and Kolter, R. 2005. Biofilms: The matrix revisited. *Trends Microbiol* 13(1): 20-25.

54. Svensson, S. L., Frirdich, E., and Gaynor, E. C. 2008. Survival strategies of *Campylobacter jejuni*: Stress responses, the viable but non-culturable state, and biofilms. In: Szymanski, C. M., Nachamkin, I., and Blaser, M. J. (Eds.) *Campylobacter*, 3rd edition. Washington, DC: ASM Press, pp. 62-85.

55. Svensson, S. L., Pryjma, M., and Gaynor, E. C. 2014. Flagella-mediated adhesion and extracellular DNA release contribute to biofilm formation and stress tolerance of *Campylobacter jejuni*. *PLoS ONE* 9(8): e106063.

56. Buswell, C. M., Herlihy, Y. M., Lawrence, L. M., McGuiggan, J. T. M., Marsh, P. D., Keevil, C. W., and Leach, S. A. 1998. Extended survival and persistence of *Campylobacter* spp. In water and aquatic biofilms and their detection by immunofluorescent-antibody and -rRNA staining. *Appl Environ Microbiol* 64(2): 733-741.

57. McLennan, M. K., Ringoir, D. D., Frirdich, E., Svensson, S. L., Wells, D. H., Jarrell, H., Szymanski, C. M., and Gaynor, E. C. 2008. *Campylobacter jejuni* biofilms up-regulated in the absence of the stringent response utilize a calcofluor white-reactive polysaccharide. *J Bacteriol* 190(3): 1097-1107.

58. Reuter, M., Mallett, A., Pearson, B. M., and van Vliet, A. H. M. 2010. Biofilm formation by *Campylobacter jejuni* is increased under aerobic conditions. *Appl Environ Microbiol* 76(7): 2122-2128.

59. Nguyen, D., Joshi-Datar, A., Lepine, F., Bauerle, E., Olakanmi, O., Beer, K., McKay, G., Siehnel, R., Schafhauser, J., Wang, Y., Britigan, B. E., and Singh, P. K. 2011. Active starvation responses mediate antibiotic tolerance in biofilms and nutrient-limited bacteria. *Science*. 334: 982-986.

60. Asakura, H., Yamasaki, M., Yamamoto, S., and Igimi, S. 2007. Deletion of *peb4* gene impairs cell adhesion and biofilm formation in *Campylobacter jejuni*. *FEMS Microbiol Lett* 275: 278-285.

61. Joshua, G. W. P., Guthrie-Irons, C., Karlyshev, A. V., and Wren, B. V. 2006. Biofilm formation in *Campylobacter jejuni*. *Microbiology* 152: 387-396.

62. Lehtola, M. J., Pitkänen, T., Miebach, L., and Miettinen, I. T. 2006. Survival of *Campylobacter jejuni* in potable water biofilms: A comparative study with different detection methods. *Water Sci Technol* 54(3): 57-61.

63. Sanders, S. Q., Boothe, D. H., Frank, J. F., and Arnold, J. W. 2007. Culture and detection of *Campylobacter jejuni* within mixed microbial populations of biofilms on stainless steel. *J Food Prot* 70(6): 1379-1385.

64. Trachoo, N., Frank, J. F., and Stern, N. J. 2002. Survival of *Campylobacter jejuni* in biofilms isolated from chicken houses. *J Food Prot* 65(7): 1110-1116.

65. Trachoo, N., and Frank, J. F. 2002. Effectiveness of chemical sanitizers against *Campylobacter jejuni*-containing biofilms. *J Food Prot* 65(7): 1117-1121.

66. Naito, M., Frirdich, E., Fields, J. A., Pryjma, M., Li, J., Cameron, A., Gilbert, M., Thompson, S. A., and Gaynor, E. C. 2010. Effects of sequential *Campylobacter jejuni* 81-176 lipooligosaccharide core truncations on biofilm formation, stress survival, and pathogenesis. *J Bacteriol* 192(8): 2182-2192.

67. Chiang, S. L., Taylor, R. K., Koomey, M., and Mekalanos, J. J. 1995. Single amino acid substitutions in the N-terminus of *Vibrio cholerae* TcpA affect colonization, autoagglutination, and serum resistance. *Mol Microbiol* 17(6): 1133-1142.

68. Menozzi, F. D., Boucher, P. E., Riveau, G., Gantiez, C., and Locht, C. 1994. Surface-associated filamentous hemagglutinin induces autoagglutination of *Bordetella pertussis*. *Infect Immun* 62(10): 4261-4269.

69. Swanson, J., Kraus, S. J., and Gotschlich, E. C. 1971. Studies on gonococcus infection. *J Exp Med* 134: 886-906.

70. Laird, W. J., and Cavanaugh, D. C. 1980. Correlation of autoagglutination and virulence of Yersiniae. *J Clin Microbiol* 11(4): 430-432.

71. Janda, J. M., Oshiro, L. S., Abbott, S. L., and Duffey, P. S. 1987. Virulence markers of the mesophilic aeromonads: Association of the autoagglutination phenomenon with mouse pathogenicity and the presence of a peripheral cell-associated layer. *Infect Immun* 55(12): 3070-3077.

72. Paula, S. J., Duffey, P. S., Abbott, S. L., Kokka, R. P., Oshiro, L. S., Janda, J. M., Shimada, T., and Sakazaki, R. 1988. Surface properties of autoagglutinating aeromonads. *Infect Immun* 56(10): 2658-2665.

73. Kokka, R. P., and Janda, J. M. 1990. Isolation and identification of autoagglutinating serogroup O:11 *Aeromonas* strains in the clinical laboratory. *J Clin Microbiol* 28(6): 1297-1299.

74. Misawa, N., and Blaser, M. J. 2000. Detection and characterization of autoagglutination activity by *Campylobacter jejuni*. *Infect Immun* 68(11): 6168-6175.

75. Skurnik, M., Bölen, I., Heikkinen, H., Piha, S., and Wolf-Watz, H. 1984. Virulence plasmid-associated autoagglutination in *Yersinia* spp. *J Bacteriol* 158(3): 1033-1036.

76. Young, K. T, Davis, L. M., and DiRita, V. J. 2007. *Campylobacter jejuni*: Molecular biology and pathogenesis. *Nat Rev Microbiol* 5: 665-679.

77. Stahl, M., Frirdich, E., Vermeulen, J., Badayeva, Y., Li, X., Vallance, B. A., and Gaynor, E. C. 2016. The helical shape of *Campylobacter jejuni* promotes *in vivo* pathogenesis by aiding transit through intestinal mucus and colonization of crypts. *Infect Immun* 84(12): 3399-3407.

78. Lertsethtakarn, P., Ottemann, K. M., and Hendrixson, D. R. 2011. Motility and chemotaxis in *Campylobacter* and *Helicobacter*. *Annu Rev Microbiol* 65: 389-410.

79. Ferrero, R. L., and Lee, A. 1988. Motility of *Campylobacter jejuni* in a viscous environment: Comparison with conventional rod-shaped bacteria. *J Gen Microbiol* 134: 53-59.

80. Dworkin, J. 2010. Form equals function? Bacterial shape and its consequences in pathogenesis. *Mol Microbiol* 78(4): 792-795.

81. Young, K. D. 2006. The selective value of bacterial shape. *Microbiol Mol Biol Rev* 70(3): 660-703.

82. Hendrixson, D. R., and DiRita, V. J. 2004. Identification of *Campylobacter jejuni* genes involved in commensal colonization of the chick gastrointestinal tract. *Mol Microbiol* 52(2): 471-484.

83. Stahl, M., Ries, J., Vermeulen, J., Yang, H., Sham, H. P., Crowley, S. M., Badayeva, Y., Turvey, S. E., Gaynor, E. C., Li, X., and Vallance, B. A. 2014. A novel mouse model of *Campylobacter jejuni* gastroenteritis reveals key pro-inflammatory and tissue protective roles for toll-like receptor signaling during infection. *PLoS Pathog* 10(7): e1004264.

84. Hermans, D., Van Deun, K., Martel, A., Van Immerseel, F., Messens, W., Heyndrickx, M., Haesebrouk, F., and Pasmans, F. 2011. Colonization factors of *Campylobacter jejuni* in the chicken gut. *Vet Res* 42: 82.

85. Wassenaar, T. M., van der Zeijst, B. A. M., Ayling, R., and Newell, D. G. 1993. Colonization of chicks by motility mutants of *Campylobacter jejuni* demonstrates the importance of flagellin A expression. *J Gen Microbiol* 139: 1171-1175.

86. Yao, R., Burr, D. H., Doig, P., Trust, T. J., Niu, H., and Guerry, P. 1994. Isolation of motile and non-motile insertional mutants of *Campylobacter jejuni*: the role of motility in adherence and invasion of eukaryotic cells. *Mol Microbiol* 14(5): 883-893.

87. Backert, S., and Hofreuter, D. 2013. Molecular methods to investigate adhesion, transmigration, invasion and intracellular survival of the foodborne pathogen *Campylobacter jejuni*. *J Microbiol Methods* 95: 8-23.

88. Mertins, S., Allan, B. J., Townsend, H. G., Köster, W., and Potter, A. A. 2013. Role of *motAB* in adherence and internalization in polarized Caco-2 cells and in cecal colonization of *Campylobacter jejuni*. *Avian Dis* 57:116-122.

89. Reeser, R. J., Medler, R. T., Billington, S. J., Jost, B. H., and Joens, L. A. 2007. Characterization of *Campylobacter jejuni* biofilms under defined growth conditions. *Appl Environ Microbiol* 73(6): 1908-1913.

90. Kalmokoff, M., Lanthier, P., Tremblay, T.-L., Foss, M., Lau, P. C., Sanders, G., Austin, J., Kelly, J., and Szymanski, C. M. 2006. Proteomic analysis of *Campylobacter jejuni* 11168 biofilms reveals a role for the motility complex in biofilm formation. *J Bacteriol* 188(12): 4312-4320.

91. Vollmer, W., and Seligman, S. J. 2010. Architecture of peptidoglycan: More data and more models. *Trends Microbiol* 18(2): 59-66.

92. Vollmer, W., Blanot, D., and de Pedro, M. A. 2008. Peptidoglycan structure and architecture. *FEMS Microbiol Rev* 32: 149-167.

93. Amano, K., and Shibata, Y. 1992. Structural studies of peptidoglycans in *Campylobacter* species. *Microbiol Immunol* 36(9): 961-967.

94. Vollmer, W., Joris, B., Charlier, P., and Foster, S. 2008. Bacterial peptidoglycan (murein) hydrolases. *FEMS Microbiol Rev* 32: 259-286.

95. Frirdich, E., and Gaynor, E. C. 2013. Peptidoglycan hydrolases, bacterial shape, and pathogenesis. *Curr Opin Microbiol* 16: 767-778.

96. Typas, A., Banzhaf, M., Gross, C. A., and Vollmer, W. 2012. From the regulation of peptidoglycan synthesis to bacterial growth and morphology. *Nat Rev Microbiol* 10: 123-136.

97. Ha, R., Frirdich, E., Sychantha, D., Biboy, J., Taveirne, M. E., Johnson, J. G., DiRita, V. J., Vollmer, W., Clarke, A. J., and Gaynor, E. C. 2016. Accumulation of peptidoglycan *O*-acetylation leads to altered cell wall biochemistry and negatively impacts pathogenesis factors of *Campylobacter jejuni*. *J Biol Chem* 291(43): 22686-22702.

98. Frirdich, E., Vermeulen, J., Biboy, J., Soares, F., Taveirne, M. E., Johnson, J. G., DiRita, V. J., Girardin, S. E., Vollmer, W., and Gaynor, E. C. 2014. Peptidoglycan LD-carboxypeptidase Pgp2 influences *Campylobacter jejuni* helical cell shape and pathogenic properties and provides the substrate for the DL-carboxypeptidase Pgp1. *J Biol Chem* 289(12): 8007-8018.

99. Frirdich, E., Biboy, J., Pryjma, M., Lee, J., Huynh, S., Parker, C. T., Girardin, S. E., Vollmer, W., and Gaynor, E. C. 2019. The *Campylobacter jejuni* helical to coccoid transition involves changes to peptidoglycan and the ability to elicit an immune response. *Mol Microbiol* 112(1): 280-301.

100. Gaynor, E. C., Cawthraw, S., Manning, G., MacKichan, J. K., Falkow, S., and Newell, D. G. 2004. The genome-sequenced variant of *Campylobacter jejuni* NCTC 11168 and the original clonal clinical isolate differ markedly in colonization, gene expression and virulence-associated phenotypes. *J Bacteriol* 186(2): 503-517.

101. Griffiths, P. L. 1993. Morphological changes of *Campylobacter jejuni* growing in liquid culture. *Lett Appl Microbiol* 17: 152-155.

102. Jackson, D. N., Davis, B., Tirado, S. M., Duggal, M., van Frankenhuyzen, J. K., Deaville, D., Wijesinghe, M. A. K., Tessaro, M., and Trevors, J. T. 2009. Survival mechanisms and culturability of *Campylobacter jejuni* under stress conditions. *Antonie Leeuwenhoek* 96: 377-394.

103. Ikeda, N., and Karlyshev, A. V. 2012. Putative mechanisms and biological role of coccoid form formation in *Campylobacter jejuni*. *Eur J Microbiol Immunol* 2: 41-49.

104. Cameron, A., Frirdich, E., Huynh, S., Parker, C. T., and Gaynor, E. C. 2012. Hyperosmotic stress response of *Campylobacter jejuni*. *J Bacteriol* 194(22): 6116-6130.

105. Uehara, T., Dinh, T., and Bernhardt, T. G. 2009. LytM-domain factors are required for daughter cell separation and rapid ampicillin-induced lysis in *Escherichia coli*. *J Bacteriol* 191(16): 5094-5107.

106. den Blaauwen, T., de Pedro, M. A., Nguyen-Disèche, M., and Ayala, J. A. 2008. Morphogenesis of rod-shaped sacculi. *FEMS Microbiol Rev* 32: 321-344.

107. Möll, A., Dörr, T., Alvarez, L., Chao, M. C., Davis, B. M., Cava, F., Waldor, M. K. 2014. Cell separation in *Vibrio cholerae* is mediated by a single amidase whose action is modulated by two nonredundant activators. *J Bacteriol* 196(22): 3937-3948.

108. Chaput, C., Ecobichon, C., Cayet, N., Girardin, S. E., Werts, C., Guadagnini, S., Prévost, M.-C., Mengin-Lecreulx, D., Labigne, A., and Boneca, I. G. 2006. Role of AmiA in the morphological transition of *Helicobacter pylori* and in immune escape. *PLoS Pathog* 2(9): e97.

109. Heidrich, C., Templin, M. F., Ursinus, A., Merdanovic, M., Berger, J., Schwarz, H., de Pedro, M. A., and Höltje, J.-V. 2001. Involvement of *N*-acetylmuramyl-L-alanine amidases in cell separation and antibiotic-induced autolysis of *Escherichia coli*. *Mol Microbiol* 41(1): 167-178.

110. Priyadarshini, R., de Pedro, M. A., and Young, K. D. 2007. Role of peptidoglycan amidases in the development and morphology of the division septum in *Escherichia coli*. *J Bacteriol* 189(14): 5334-5347.

111. Uehara, T., Parzych, K. R., Dinh, T., and Bernhardt, T. G. 2010. Daughter cell separation is controlled by cytokinetic ring-activated cell wall hydrolysis. *EMBO J* 29: 1412-1422.

112. Firczuk, M., and Bochtler, M. 2007. Folds and activities of peptidoglycan amidases. *FEMS Microbiol Rev* 31: 676-691.

113. Finn, R. D., Tate, J., Mistry, J., Coggill, P. C., Sammut, S. J., Hotz, H.-R., Ceric, G., Forslund, K., Eddy, S. R., Sonnhammer, E. L. L., and Bateman, A. 2008. The Pfam protein families database. *Nucleic Acids Res* 36: D281-D288.

114. Möll, A., Schlimpert, S., Briegel, A., Jensen, G. J., and Thanbichler, M. 2010. DipM, a new factor required for peptidoglycan remodelling during cell division in *Caulobacter crescentus*. *Mol Microbiol* 77(1): 90-107.

115. Sycuro, L. K., Pincus, Z., Gutierrez, K. D., Biboy, J., Stern, C. A., Vollmer, W., and Salama, N. R. 2010. Peptidoglycan crosslinking relaxation promotes *Helicobacter pylori*'s helical shape and stomach colonization. *Cell* 141: 822-833.

116. Meisner, J., and Moran Jr., C. P. 2011. A LytM domain dictates the localization of proteins to the mother cell-forespore interface during bacterial endospore formation. *J Bacteriol* 193(3): 591-598.

117. Peters, N. T., Morlot, C., Yang, D. C., Uehara, T., Vernet, T., and Bernhardt, T. G. 2013. Structure-function analysis of the LytM domain of EnvC, an activator of cell wall remodelling at the *Escherichia coli* division site. *Mol Microbiol* 89(4): 690-701.

118. Odintsov, S. G., Sabala, I., Marcyjaniak, M., and Bochtler, M. 2004. Latent LytM at 1.3 Å resolution. *J Mol Biol* 335: 775-785.

119. Firczuk, M., Mucha, A., and Bochtler, M. 2005. Crystal structures of active LytM. *J Mol Biol* 354: 578-590.

120. Nakamura, N., Hoshino, Y., Shiga, T., Haneda, T., Okada, N., and Miki, T. 2020. A peptidoglycan amidase activator impacts *Salmonella enterica* serovar Typhimurium gut infection. *Infect Immun* 88(6): e00187-20.

121. Oguri, T., Yeo, W.-S., Bae, T., and Lee, H. 2016. Identification of EnvC and its cognate amidases as novel determinants of intrinsic resistance to cationic antimicrobial peptides. *Antimicrob Agents Chemother* 60(4): 2222-2231.

122. Yakhnina, A. A., McManus, H. R., and Bernhardt, T. G. 2015. The cell wall amidase AmiB is essential for *Pseudomonas aeruginosa* cell division, drug resistance and viability. *Mol Microbiol* 97(5): 957-973.

123. Mousavi, S., Bereswill, S., and Heimesaat, M. M. 2020. Novel clinical *Campylobacter jejuni* infection models based on sensitization of mice to lipooligosaccharide, a major bacterial factor triggering innate immune responses in human campylobacteriosis. *Microorganisms* 8: 482.

124. Haag, L.-M., Fischer, A., Otto, B., Plickert, T., Kühl, A. A., Göbel, U. B., Bereswill, S., and Heimesaat, M. M. 2012. *Campylobacter jejuni* induces acute enterocolitis in gnotobiotic IL-10$^{-/-}$ mice via toll-like-receptor-2 and -4 signaling. *PLoS ONE* 7(7): e40761.

125. Mansfield, L. S., Bell, J. A., Wilson, D. L., Murphy, A. J., Elsheikha, H. M., Rathinham, V. A. K., Fierro, B. R., Linz, J. E., and Young, V. B. 2007. C57BL/6 and congenic interleukin-10-deficient mice can serve as models of *Campylobacter jejuni* colonization and enteritis. *Infect Immun* 75(3): 1099-1115.

126. Otto, B., Haag, L.-M., Fischer, A., Plickert, R., Kühl, A. A., Göbel, U. B., Heimesaat, M. M., and Bereswill, S. 2012. *Campylobacter jejuni* induces extra-intestinal immune response via toll-like-receptor-4 signaling in conventional IL-10 deficient mice with chronic colitis. *Eur J Microbiol Immunol* 2: 210-219.

127. Sun, X., Liu, B., Sartor, R. B., and Jobin, C. 2013. Phosphatidylinositol 3-kinase-γ signalling promotes *Campylobacter jejuni* induced colitis through neutrophil recruitment in mice. *J Immunol* 190: 357-365.

128. Heimesaat, M. M., Alutis, M., Grundmann, U., Fischer, A., Tegtmeyer, N., Böhm, M., Kühl, A. A., Göbel, U. B., Backert, S., and Bereswill, S. 2014. The role of serine protease HtrA in acute ulcerative enterocolitis and extra-intestinal immune responses during *Campylobacter jejuni* infection of gnotobiotic IL-10 deficient mice. *Front Cell Infect Microbiol* 4: Article 77.

129. Karlyshev, A. V., and Wren, B. W. 2005. Development and application of an insertional system for gene delivery and expression in *Campylobacter jejuni*. *Appl Environ Microbiol* 71(7): 4004-4013.

130. Ménard, R., Sansonetti, P. J., and Parsot, C. 1993. Nonpolar mutagenesis of the *ipa* genes defines IpaB, IpaC, and IpaD as effectors of *Shigella flexneri* entry into epithelial cells. *J Bacteriol* 175(18): 5899-5906.

131. Pincus, Z., and Teriot, J. A. 2007. Comparison of quantitative methods for cell-shape analysis. *J Microsc* 227: 140-156.

132. O'Toole, G. A., and Kolter, R. 1998. Initiation of biofilm formation in *Pseudomonas fluorescens* WCS365 proceeds via multiple, convergent signalling pathways: A genetic analysis. *Mol Microbiol* 28(3): 449-461.

133. Rosenberg, M., Gutnick, D., and Rosenberg, E. 1980. Adherence of bacteria to hydrocarbons: A simple method for measuring cell surface hydrophobicity. *FEMS Microbiol Lett* 9: 29-33.

134. Nguyen, V. T., Turner, M. S., and Dykes, G. A. 2011. Influence of cell surface hydrophobicity on attachment of *Campylobacter* to abiotic surfaces. *Food Microbiol* 28: 942-950.

135. Chaput, C., Ecobichon, C., Pouradier, N., Rousselle, J.-C., Namane, A., and Boneca, I. G. 2016. Role of the *N*-acetylmuramoyl-L-alanyl amidase, AmiA, of *Helicobacter pylori* in peptidoglycan metabolism, daughter cell separation, and virulence. *Microb Drug Resist* 22(6): 477-486.

136. Wood, P. J. 1980. Specificity in the interaction of direct dyes with polysaccharides. *Carbohydr Res* 85: 271-287.

137. Solano, C., García, B., Valle, J., Berasain, C., Ghigo, J.-M., Gamazo, C., and Lasa, I. 2002. Genetic analysis of *Salmonella enteritidis* biofilm formation: Critical role of cellulose. *Mol Microbiol* 43(3): 793-808.

138. Ledeboer, N. A., and Jones, B. D. 2005. Exopolysaccharide sugars contribute to biofilm formation by *Salmonella enterica* serovar Typhimurium on Hep-2 cells and chicken intestinal epithelium. *J Bacteriol* 187(9): 3214-3226.

139. Zogaj, X., Nimtz, M., Rohde, M., Bokranz, W., and Römling, U. 2001. The multicellular morphotypes of *Salmonella typhimurium* and *Escherichia coli* produce cellulose as the second component of the extracellular matrix. *Mol Microbiol* 39(6): 1452-1463.

140. Howard, S. L., Jagannathan, A., Soo, E. C., Hui, J. P. M., Aubry, A. J., Ahmed, I., Karlyshev, A., Kelly, J. F., Jones, M. A., Stevens, M. P., Logan, S. M., and Wren, B. W. 2009. *Campylobacter jejuni* glycosylation island important in cell charge, legionaminic acid biosynthesis, and colonization of chicks. *Infect Immun* 77(6): 2544-2556.

141. Rathbun, K. M., and Thompson, S. A. 2009. Mutation of PEB4 alters the outer membrane protein profile of *Campylobacter jejuni*. *FEMS Microbiol Lett* 300: 188-194.

142. Matsukawa, M., and Greenberg, E. P. 2004. Putative exopolysaccharide synthesis genes influence *Pseudomonas aeruginosa* biofilm development. *J Bacteriol* 186(14): 4449-4456.

143. Heidrich, C., Ursinus, A., Berger, J., Schwarts, H., and Höltje, J.-V. 2002. Effects of multiple deletions of murein hydrolases on viability, septum cleavage, and sensitivity to large toxic molecules in *Escherichia coli*. *J Bacteriol* 184(22): 6093-6099.

144. Montanaro, L., Poggi, A., Visai, L, Ravaioli, S., Campoccia, D., Speziale, P., and Arciola, C. R. 2011. Extracellular DNA in biofilms. *Int J Artif Organs* 34(9): 824-831.

145. Thomas, V. C., Thurlow, L. R., Boyle, D., and Hancock, L. E. 2008. Regulation of autolysis-dependent extracellular DNA release by *Enterococcus faecalis* extracellular proteases influences biofilm development. *J Bacteriol* 190(16): 5690-5698.

146. Mulcahy, H., Charron-Mazenod, L., and Lewenza, S. 2008. Extracellular DNA chelates cations and induces antibiotic resistance in *Pseudomonas aeruginosa* biofilms. *PLoS Pathog* 4(11): e1000213.

147. Cook, J., Baverstock, T. C., McAndrew, M. B. L., Stansfeld, P., Roper, D. I., and Crow, A. 2020. Insights into bacterial cell division from a structure of EnvC bound to the FtsX periplasmic protein. *PNAS* 117(45): 28355-28365.

148. Klöckner, A., Otten, C., Derouaux, A., Vollmer, W., Bühl, H., De Benedetti, S., Münch, D., Josten, M., Mölleken, K., Sahl, H.-G., and Henrichfreise, B. 2014. AmiA is a penicillin target enzyme with dual activity in the intracellular pathogen *Chlamydia pneumoniae*. *Nat Commun* 5: 4201.

149. Pichoff, S., Du, S., and Lutkenhaus, J. 2019. Roles of FtsEX in cell division. *Res Microbiol* 170: 374-380.

150. Mavrici, D., Marakalala, M. J., Holton, J. M., Prigozhin, D. M., Gee, C. L., Zhang, Y. J., Rubin, E. J., and Alber, T. 2014. *Mycobacterium tuberculosis* FtsX extracellular domain activates the peptidoglycan hydrolase, RipC. *PNAS* 111(22): 8037-8042.

151. Yang, D. C., Peters, N. T., Parzych, K. R., Uehara, T., Markovski, M., and Bernhardt, T. G. 2011. An ATP-binding cassette transporter-like complex governs cell-wall hydrolysis at the bacterial cytokinetic ring. *PNAS* 108(45): E1052-E1060.

152. Yang, L.-C., Gan, Y.-L., Yang, L.-Y., Jiang, B.-L., and Tang, J.-L. 2018. Peptidoglycan hydrolysis mediated by the amidase AmiC and its LytM activator NlpD is critical for cell separation and virulence in the phytopathogen *Xanthomonas campestris. Mol Plant Pathol* 19(7): 1705-1718.

153. Kuru, E., Hughes, H. V., Brown, P. J., Hall, E., Tekkam, S., Cava, F., de Pedro, M. A., Brun, Y. V., and VanNieuwenhze, M. S. 2012. In situ probing of newly synthesized peptidoglycan in live bacteria with fluorescent D-amino acids. *Agnew Chem Int Ed* 51: 12519-12523.

Appendix A

Appendix A.1 Supplementary Figures and Tables

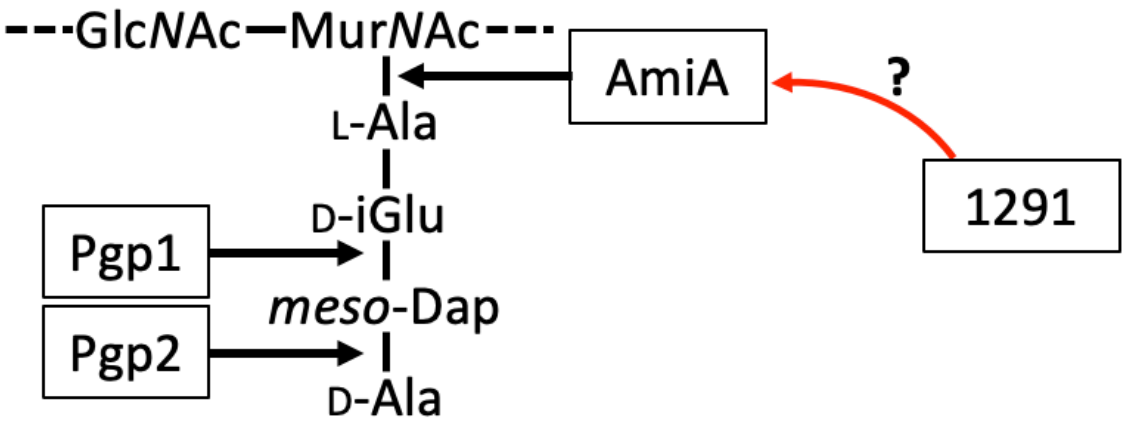

Figure A.1.1 Schematic diagram of *C. jejuni* PG. The cleavage sites of carboxypeptidases Pgp1, which hydrolyzes tripeptides (39), and Pgp2, which hydrolyzes tetrapeptides (98), and the LytC-type *N*-acetylmuramoyl-L-alanine amidase AmiA, which cleaves the peptide side chain from the glycan backbone (99), are indicated with a black arrow. The putative activation of AmiA by 1291 is indicated by a red arrow. Glc*N*Ac, *N*-acetylglucosamine; Mur*N*Ac, *N*-acetylmuramic acid; Ala, alanine; iGlu, isoglutamic acid; *meso*-Dap, *meso*-diaminopimelic acid.

Table A.1.1 Codon differences between native *Cj 1291* and *1291CO*. *1291CO* was optimized for *E. coli* expression using Integrated Gene Technologies' online codon optimization tool.

		Codon	
Amino acid	**Amino acid residue**	***1291***	***1291CO***
Alanine (A)	20, 313	GCA	GCG
	22, 276	GCT	GCC
	48, 79, 81, 134, 168, 206, 333	GCT	GCA
	77, 209	GCA	GCC
	112, 182	GCT	GCG
	185, 326, 368	GCC	GCG
	349	GCA	GCT
Cysteine (C)	10	TGT	TGC
Aspartic acid (D)	16, 50, 95, 118, 179, 204, 213, 214, 234, 237, 279, 312, 320, 328, 341, 376	GAT	GAC
Glutamic acid (E)	25, 38, 45, 66, 76, 94, 127, 147, 148, 175, 220, 380	GAA	GAG
	157, 221, 302	GAG	GAA
Phenylalanine (F)	8, 11, 14, 135, 150, 281, 287, 300, 386	TTT	TTC
Glycine (G)	139, 263, 271, 288	GGA	GGG
	158	GGG	GGA
	258, 371	GGT	GGA
	343	GGC	GGA
	367	GGT	GGG
	361	GGT	GGC
Histidine (H)	345, 387	CAT	CAC
Isoleucine (I)	7, 388	ATC	ATT
	17, 36, 108, 207, 247	ATA	ATC
	23, 254, 275, 323, 344, 347, 373	ATA	ATT
	51, 65, 232, 354, 358, 394	ATT	ATC
Lysine (K)	3, 28, 42, 43, 56, 59, 74, 100, 151, 154, 178, 191, 193, 224, 242, 249, 298, 316, 322, 359, 362, 366	AAA	AAG
Leucine (L)	6, 75, 89, 97, 107, 177, 297	CTT	CTG
	44, 162, 377	CTT	TTA
	61	CTA	CTT
	68, 86, 119, 190, 229, 306	TTA	CTG
	96, 278	TTG	CTT
	141, 184	TTA	CTT
	212, 393	CTC	CTT
	215, 391	TTG	TTA
	319	CTA	TTG
	332, 351, 396	TTA	TTG

Amino acid	Amino acid residue	Codon	
		1291	*1291CO*
Asparagine (N)	24, 33, 41, 93, 102, 146, 174, 233, 239, 250, 296, 303, 309, 317, 357, 363, 385, 389, 397	AAT	AAC
	199	AAT	AAC
	181, 241	AAC	AAT
Proline (P)	120, 122	CCT	CCA
	277	CAA	CCG
	293	CCT	CCG
	390	CCT	CCC
Glutamine (Q)	39, 169	CAG	CAA
	71, 84, 123, 167, 188, 192, 201, 256	CAA	CAG
Arginine (R)	2, 223, 255, 307, 372	AGA	CGT
	161	AGG	CGT
	205	CGA	CGT
	268	CGT	CGC
	334	CGA	CGC
Serine (S)	18, 57, 131, 140, 330	AGT	TCC
	29, 78	AGT	TCT
	49, 67	AGC	TCG
	62, 311	AGT	TCA
	70	TCA	TCG
	73	TCT	TCG
	91	AGC	TCT
	101, 265	TCA	AGC
	109, 280	TCT	TCA
	153	TCT	AGC
	160, 308	AGC	TCC
	196	AGC	AGT
	240	TCA	TCT
	259	TCA	ACT
	260	AGC	TCA
	264	AGT	TCG
	395	AGC	TCG
Threonine (T)	27, 225, 346	ACA	ACG
	72, 382	ACT	ACC
	90, 235	ACA	ACT
	203	ACA	ACC
	245, 378	ACT	ACA
	274	ACC	ACG

Amino acid	Amino acid residue	Codon	
		1291	*1291CO*
Threonine (T)	282, 329	ACT	ACG
Valine (V)	15, 291, 324	GTT	GTA
	144, 294, 315, 338, 360	GTT	GTC
	159, 304, 381	GTA	GTC
	248	GTA	GTT
	266	GTC	GTT
	283, 370	GTG	GTT
	314, 335	GTT	GTG
	318	GTG	GTA
	369	GTA	GTG
Tyrosine (Y)	117, 125, 208, 261	TAT	TAC
	180	TAC	TAT
Stop codon	398	TAG	TAA

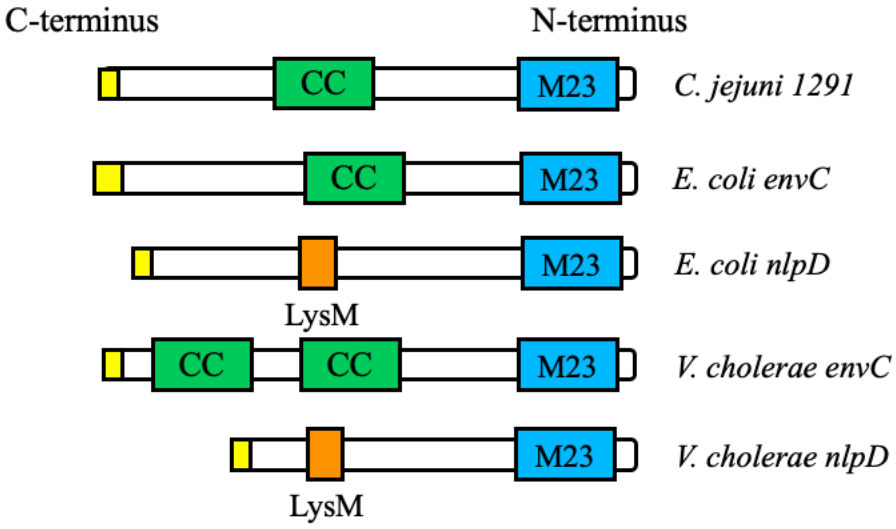

Figure A.1.2 The predicted gene domains of *Cj* Δ*1291* and the amidase activators *envC* and *nlpD* from *E. coli* and *V. cholerae* as determined by E. Frirdich and J. Wallace. The yellow domain at the C-terminal end represents the signal peptide, the coiled coil regions are shown by the green CC box, the orange domains are PG binding LysM domains, and the M23 peptidase (LytM) domain is represented by the blue M23 box.

Figure A.1.3 Amino acid alignment of *Cj* 1291 and *E. coli* EnvC. The alignment of *Cj* 1291 (Cj_1291) and *E. coli* EnvC (Ec_EnvC) was generated using the free online software Clustal Omega. The signal peptides in each protein are underlined. Coiled coil regions are coloured green, and the LytM domains are coloured blue. Residues involved in EnvC-amidase binding are red (117). The yellow highlighted 1291 residues are amino acids that may be important in 1291-amidase binding.

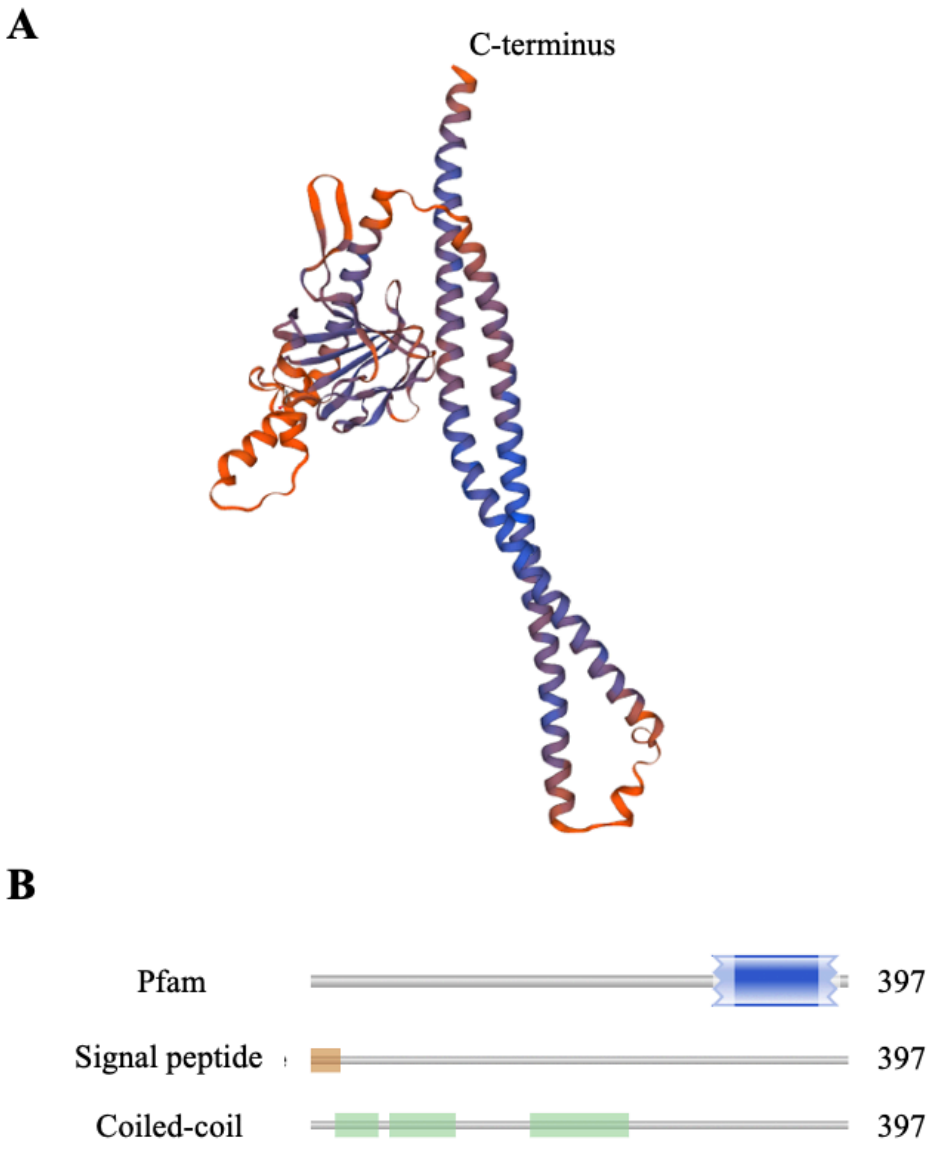

Figure A.1.4 Predicted 1291 protein structure. A) The predicted three-dimensional structure of *Cj* 1291 determined using the free online Swiss-Model software shows the three coiled coil regions predicted to be present by the B) protein domain analysis completed using the free online program HMMER. In A) the blue to red gradient shows the confidence with blue and red indicating high and low confidence, respectively.

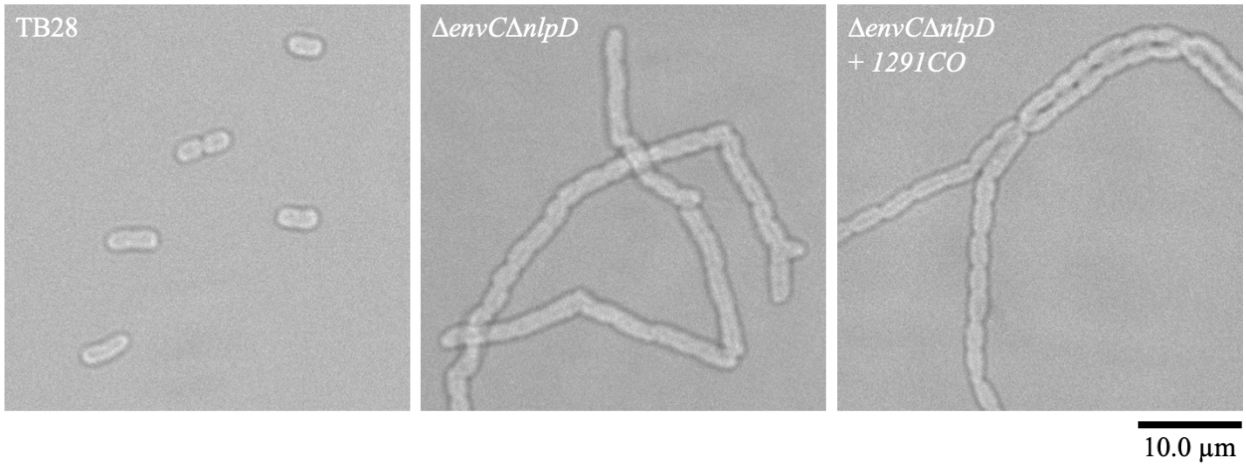

Figure A.1.5 Cellular morphology of *E. coli* Δ*envC*Δ*nlpD* expressing the codon optimized *1291* gene in the pRRC plasmid grown without chloramphenicol. Cells were imaged by DIC microscopy at 100X magnification. The Δ*envC*Δ*nlpD* + *1291CO* strain was grown for four hours in LB broth with no supplemental antibiotics.